UiO : Department of Physics
University of Oslo

Parametrization of the nightside reconnection rate during times with contracting polar caps

Sondre Øye

Master's Thesis, Spring 2018

This master's thesis is submitted under the master's program *Lektorprogrammet*, with program option *Physics*, at the Department of Physics, University of Oslo. The scope of the thesis is 30 credits.

The front page depicts a selection of formula that a student in space physics might encounter.

Abstract

Determining the nightside reconnection rate is an integral part in determining high-latitude convection. Obtaining a way to predict the nightside reconnection rate will therefore be an important step toward developing a way to forecast space weather. Using a time series of the open magnetic flux in the polar caps (F_{PC}) derived from the Active Magnetospheric and Planetary Electrodynamic Response Experiment (AMPERE) and interplanetary parameters from OMNI, I parameterize the nightside reconnection rate during times with contracting polar caps. This is done both directly by using Faraday's equation and by parametrizing the change in F_{PC}. The maximum correlation between predicted and observed nightside reconnection rates exceeds 0.85, however, it is found that an independent trigger is needed to tell when the nightside reconnection starts and ends.

Acknowledgements

I acknowledge use of NASA/GSFC's Space Physics Data Facility's OMNIWeb service, and OMNI data.

I also want to thank the AMPERE team and the AMPERE Science Center for providing the Iridiumderived data products.

A special thanks my supervisor Lasse Clausen for all the help during this work, and for providing magnetic flux data for the polar caps.

I would also like thank friend and fellow student Audun Solberg, I've learned a lot from our weird discussions of physics.

Contents

List of Figures

List of Tables

CHAPTER 1

Introduction

1.1 Motivation

With continuous strides in technology and automation of several tasks, understanding the underlying limitations of these technologies becomes of utmost importance. One area with huge strides in automation the last decades, and with more to come, is transportation. A prime example being the aviation industry where satellite tracking has greatly increased the efficiency of the industry. Most commercial flights are flown by the autopilot, which among other things is fed with position data from satellites. This allows the space between planes to safely be shortened, reducing the pilots' workload to takeoff and landing, and turning on the autopilot for the rest of the flight. Similarly, one hopes that "self-driving" cars can help make traffic safer and more efficient in the same way.

The question then becomes how good is the position data obtained from satellites, when are they trustworthy and when are they not? The position is found by triangulating the distance to four or more satellites. These distances can contain errors from multiple sources, e.g. clock errors (satellite and receiver), orbit height error, multipath, receiver noise, tropospheric signal delay and ionospheric signal delay. Of these, the ionospheric signal delay is largest. The ionospheric signal delay is due to the fact that the propagation speed of EM-signals is reduced when traveling through dispersive media, like the ionosphere. At times the ionospheric signal delay can be so severe that scintillations in the carrier phase and fading of the signal causes loss of lock, where the receiver is no longer able to track the satellite signal. Most charged particles are found in the ionosphere located in heights between 50km and 1000km. The highest densities of charged particles in the ionosphere are found over the equator and at high latitudes. Both places have strong current systems, and these currents intensifies in times of magnetic storms (Misra and Enge, 2010; Prölss and Bird, 2004). So we want to develop a method to forecast space weather, the movement an densities of plasma in the ionosphere, in order to get a handle on this type of error in satellite communication. This thesis will focus on the magnetic nightside reconnection, as a piece in the larger puzzle that space weather is.

1.2 Theory

Dungey (1961) was the first to propose magnetic reconnection in the dayside magnetopause current sheet, a phenomena that later has been linked to the ionospheric currents. The magnetopause being the boundary between the geomagnetic field, magnetic field lines with footprints on Earth making up the magnetosphere, and the interplanetary magnetic field (IMF). Magnetic reconnection is a process, where two opposite pointing magnetic field lines are spliced to form two new field lines with a different configuration. This theory gained traction when Pioneer V discovered the existence of a regular interplanetary magnetic field. With the IMF present, the geomagnetic field had something to reconnect with. That allows energy, mass, and momentum to be transferred from the solar wind (SW) into the magnetosphere. As the SW travels at supersonic velocities a bow shock is formed around the Earth's magnetosphere. This funnels the plasma in the SW between the bow shock and magnetopause, creating the magnetosheath. When the plasma in the magnetosheath flows through the magnetic field over the poles the charges separate, and a surplus of positive charges end up one the dawn side and negative charges on the dusk side. Which creates the two cells electrical potential that is predicted by Dungey (1961). This induces an electric dynamo field, which also propagates down into the ionosphere (Prölss and Bird, 2004). With both an electrical field and a magnetic field in the ionosphere the plasma there will move as a result of $\vec{E} \times \vec{B}$-drift (eq. 1.6), and a flow along equipotential lines for cells are created.

High in the ionosphere the drift does not cause any currents as there is no net transport of charges. However, as one gets lower down in the ionosphere the concentrations of neutrals steadily increase, leading to an increased collision frequency between the plasma and the neutrals. Due to the weight difference between the light electrons and the heavy ions, the collisions lead to currents as the electrons outrace the relatively immobile ions. This creates the Hall current (red arrows in fig. 1.1), which follows the equipotential lines going opposite two the plasma flow, as well as the Pedersen currents (green arrows in fig. 1.1) going along the electrical field (Prölss and Bird, 2004). Both these currents are shown in figure 1.1. Looking at figure 1.1. one notices that the Hall currents form a closed circuit, but the Pedersen currents do not. To get a closed circuit for the Pedersen current, field aligned currents (FAC) are needed. Those currents are the Birkeland region 1 and region 2 currents. The Birkeland region 2 current goes up from the polar oval on the dawn side and connects to the ring current in the equatorial plane, before it comes down again to the polar oval on the dusk side. The region 1 currents goes up from the open closed boundary (OCB) at the dusk side and connects to the magnetopause current before it comes down to the OCB again at the dawn side.

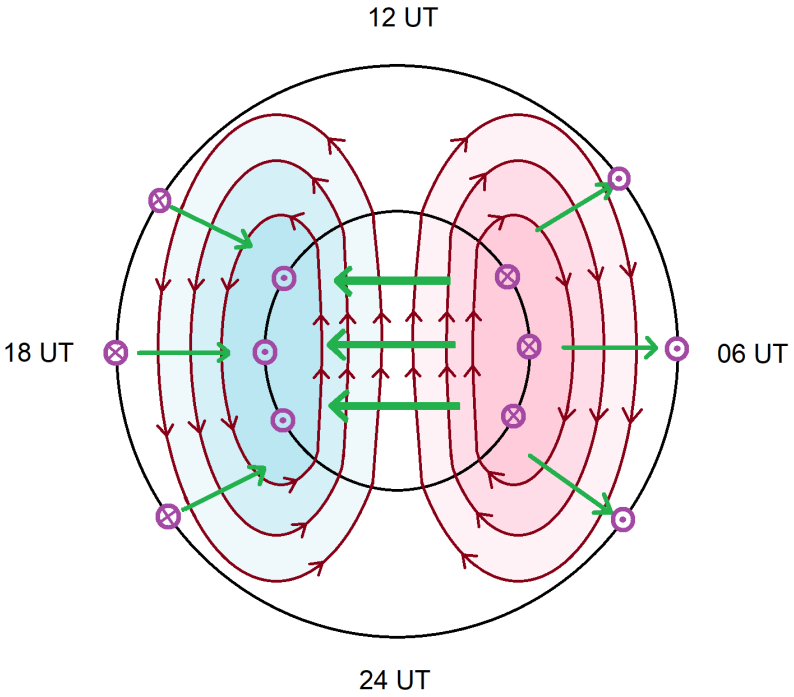

Figure 1.1: The ionospheric currents, Hall currents following the equipotential lines of the two potential cells, opposite two the plasma flow. Pedersen currents following the electric fields, away from the dawn cell and towards dusk cell. Birkeland currents, Region 2 up from auroral oval (outer circle) on the dawn side and down on it at dusk. Region 1 up from the OCB (inner circle) at dusk, and down on it on the dawn side.

Field lines in the geomagnetic field can be divided into two categories; open and closed field lines. A closed field line has both ends connected to the Earth. An open field line is on the other hand just connected to the Earth on one end, the other stretching outward in an area dubbed the magnetotail and eventually connecting to the interplanetary medium and the Sun. The footprints of the open field lines are centered around the magnetic pole, this area is dubbed the polar cap. The open closed boundary (OCB) is, as the name then would suggest, the boundary between the open and closed field lines. Dungey (1961) describes how the magnetic field lines flow into and out of the polar cap, in a cycle later dubbed the Dungey Cycle. Figure 1.2 shows this cycle for a field line. It begins with a southward pointing IMF ($B_z < 0$) coming towards the Earth (t_1). After passing the Bow shock and traveling through the magnetosheath, it hits the magnetopause. When the southward pointing IMF hits the magnetopause it meets the northward pointing geomagnetic field leading to magnetic reconnection, dayside reconnection, (t_2). The new open field lines, with a footprint in the polar cap,

are then pushed towards the nightside by the SW ($t_3 - t_4$). As the magnetotail is packed more and more with open magnetic flux, the field lines with footprint in the different hemispheres get closer. These are again oppositely directed and can reconnect (t_5). After the nightside reconnection the new closed field line is accelerated towards Earth, whilst the newly formed IMF line is accelerated away from Earth (t_6). As new closed field lines are formed they forced towards the dayside, with their footprints flowing along in the equipotential lines of the two cells (t_7). Eventually it arrives at the dayside and as closed field lines in front are eroded away through reconnection, it starts the cycle anew.

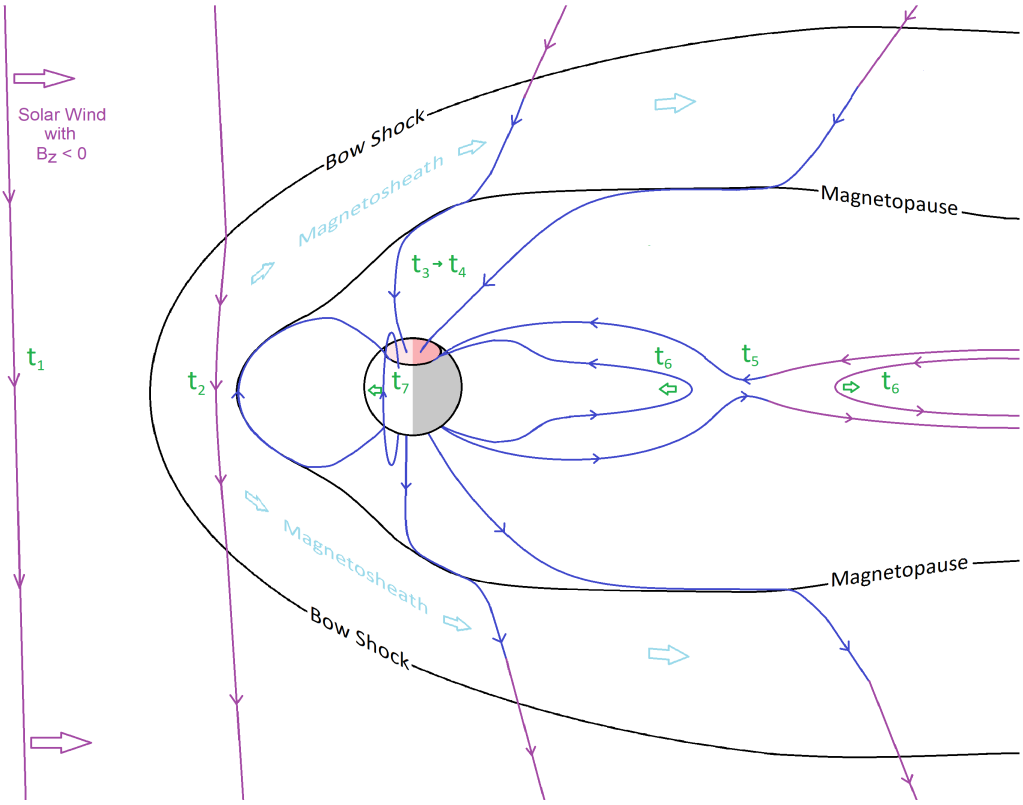

Figure 1.2: The Dungey Cycle

The interplanetary medium and the IMF mainly consists of particles from the solar wind and magnetic field trapped in the SW (Prölss and Bird, 2004). So it clear that at least the dayside reconnection is driven by the SW, which means we must understand that to predict space weather. The solar wind consists of plasma ejected by the Sun, and it is constantly hitting the magnetosphere as the Sun continually ejects matter. However, the speed and density of the SW varies massively. The speed varies from slow winds, $300 - 400$ km/s, to fast winds, $700 - 900$ km/t, and densities between dilute values at $0.1\,\mathrm{cm}^{-3}$ and dense values at $72\mathrm{cm}^{-3}$, with largest densities during coronal mass ejections (CME). CMEs are the result of large loops of the Suns magnetic field being accelerated outward by internal magnetic forces in the Sun. When these magnetic field loops are accelerated outward, they also bring with them large quantities of plasma from the Suns corona. This results in a dense SW with a strong magnetic field. The rate of the CMEs varies with the Sun's activity, and the Sun is known to have cycle of 11 years (Prölss and Bird, 2004). CMEs are of special importance as large perturbations in B_Z have been shown to coincide well with CMEs for 1 h averages, CMEs also generate longer intervals of strongly southward average IMF then calm SWs and consequently stronger geomagnetic storms (Lockwood et al., 2016). A strong southward IMF in the SW is key element that controls the level of space weather disturbances on Earth (Milan et al., 2012; Lockwood et al., 2016).

The SW can be described using Ideal Magnetohydrodynamics (MHD). One of the concepts in Ideal MHD that is applicable for the SW, is the idea of a Frozen-in-field. A Frozen-in-field means that the magnetic field lines follow the flow in the plasma (Prölss and Bird, 2004; Pécseli, 2012). So this means that an upstream measurement of the IMF parameters can be used to predict conditions at Earth.

However, when the SW hits the magnetopause the plasma becomes compacted lowering the conductivity and breaking the conditions for ideal MHD. Even though ideal MHD brakes down locally at the point of reconnection, the ends of the field lines connected in the interplanetary medium are still dragged along as described by ideal MHD.

Following Dungy's paper (1961), nightside reconnection was believed to be directly driven by the solar wind, as the dayside reconnection. This can be seen in Akasofu (1964) paper about substorms, where the substorm is divided into two phases; the expansion phase and the recovery phase. Substorms are violent signatures of the coupling between the magnetosphere and the ionosphere, where large amounts of power is released from the magnetotail in a short interval. They are identified by intense plasma flows in the plasma sheet, the buildup of strong field-aligned currents and strong energetic particle precipitation that create bright and dynamic auroras (Frey et al., 2004). Substorms thusly represent some of the strongest nightside reconnection times there are. Akasofu (1964) does not discuss the cause of substorms, but the two phases coincides with strong magnetic reconnection exciting the ionosphere and the calming after the storm. The case was soon found to be more complex than described by Akasofu (1964). In McPherron et al. (1973) the picture was slightly modified with a growth phase preceding the expansion and recovery phases. The growth phase entails the erosion of closed field lines through dayside reconnection and transport of open field lines into the magnetotail. The magnetotail being loaded with magnetic flux until the onset of the expansion phase. Where and when the onset of the expansion phase is initiated is a complex process and an expansion phase can even have multiple onsets centered at different local times (McPherron et al., 1973).

The magnetotail consists of both closed and open field lines. Closed field lines are located in the inner part "close to Earth", whilst the open field lines form two lobes that stretch far out. The lobes are connected to different hemispheres and separated by a plasma sheet called the neutralsheet. The plasma sheet is about $6\mathrm{R_E}$ thick in the center of the tail at quiet times at $16\mathrm{R_E}$ from the Earth, making it quite the barrier between the lobes. Each lobe is also surrounded by a solenoid current made up by the cross tail current in the neutral sheet and the magnetopause current (Prölss and Bird, 2004; Russell and McPherron, 1973). During substorm growth phase the tail experiences enhanced magnetic field strength in the lobes as dayside reconnection progresses, inward convection of plasma in the neutral sheet, establishment of an inward extension of the tail current or partial ring current, thinning of the neutral sheet and a strengthening of field-aligned and ionospheric currents. Eventually an onset for the expansion phase is reached, and the tail experiences strong fluctuations in the electric and magnetic fields, the energization and injection of particles close to the Earth, and rapid expansion of the neutral sheet boundaries into the lobes of the tail (McPherron et al., 1973; Russell and McPherron, 1973). The onset of substorms are not well understood, (Russell and McPherron, 1973) postulate that the onset occurs when the plasma sheet somewhere thins to zero. Other triggers for the onset may be the solar wind, an ionospheric event or a magnetospheric event. The solar wind would be most advantageous for a space weather model, but recent literature seems to have discounted it, as studies that have tried to say something about the nightside reconnection rate using the SW have not found any correlation. Like Østgaard et al. (2005) found that nightside reconnection rate correlates poorly with the solar wind electric field saying that it indicates the magnetotail reconnection to not be directly driven by the SW, but rather being an internal magnetospheric process.

Connection between space weather and Φ_N

Faraday's law states that the electromotive force ε is given by the rate of change of the magnetic flux. Applying that to the magnetic flux content of the polar cap and assuming the magnetic field over the poles to be constant, one obtains that the polar cap itself must expand and contract, changing the area (A) of the polar caps, as the ε is induced by the SW (Cowley and Lockwood, 1992; Lockwood and Cowley, 1992).

$$\varepsilon = -\frac{\mathrm{d}F_{PC}}{\mathrm{d}t} = -B_P \frac{\mathrm{d}A}{\mathrm{d}t} \tag{1.1}$$

Here B_P is the geomagnetic field over the polar caps, which can easily be modeled. F_{PC} is the open magnetic flux contained in the polar cap.

Using the model presented by Dungey (1961), we know that the open magnetic flux can either grow by dayside reconnection (Φ_D) or shrink by nightside reconnection (Φ_N). Entering these rates into eq. 1.1

and assuming the OCB be to be a circle with radius a one gets:

$$\frac{\mathrm{d}F_{PC}}{\mathrm{d}t} = \frac{\mathrm{d}}{\mathrm{d}t}|\pi a^2 B_P| = \Phi_D - \Phi_N \tag{1.2}$$

Siscoe and Huang (1985) describe how one can model the electric field and thus the various ionospheric currents by determining the electric potential Ψ in the ionosphere. With the electric potential, the electric field can be derived from Laplace's equations and in turn the flow speed and currents can be found from drift velocities. For a circular OCB the electric potential $\Psi(r, \phi)$ can be written as

$$\Psi(r, \phi) = \sum_{m=1}^{\infty} A_m \left(\frac{r}{a}\right)^{\pm m} sin(m\phi) \tag{1.3}$$

where ϕ is the angle from the noon-midnight line and r is the radius in a cylindrical coordinate system. The symmetry around the noon-midnight line makes Ψ an odd function, excluding the cosine series. The coefficients A_m are decided from the boundary conditions, i.e. Ψ value on the OCB.

$$A_m = \frac{1}{\pi} \int_0^{2\pi} \Psi(a, \phi) \sin(m\phi)\, \mathrm{d}\phi \tag{1.4}$$

To determine $\Psi(a, \phi)$ Siscoe and Huang (1985) split the OCB into two categories, adiaroic parts where the plasma cannot flow across the OCB and merging lines where the flow can cross the OCB. The interesting part for this thesis being the adiaroic lines, as those end up being dependent upon the rate of magnetic flux flowing across the merging lines Φ_{PC}, also known as the cross polar cap potential. That rate will for the dayside merging line correspond to Φ_D and for the nightside merging line correspond to Φ_N. The merging gaps are the OCB segment between the foci of the two potential cells. In figure 1.1 a time where $\Phi_D = \Phi_N >> 0$ is shown, but for a dominant Φ_D the foci would move along the OCB towards noon creating a smaller gap. The same goes for dominant Φ_N, only towards midnight. Siscoe and Huang (1985) derive that the electric potential on the OCB is:

$$\Psi(a, \phi) = \begin{cases} -\dfrac{\Phi_{PC}}{2} \dfrac{\pi - \phi}{\pi - \alpha} & \alpha < \phi < 2\pi - \alpha \\ \displaystyle\sum_{k=0}^{\infty} B_{2k+1} \left(\frac{\phi}{\alpha}\right)^{2k+1} & -\alpha < \phi < \alpha \end{cases} \tag{1.5}$$

where α is the half width angle for the merging gap.

So if the dayside and nightside reconnection rates can be predetermined, so can the electric potential be determined in advance as well. Then we have a way to predict the electric field, as it is given by Laplace's equation. Since the magnetic field is already modeled, the plasma can flow be found from

$$\vec{v}_D = \frac{\vec{E} \times \vec{B}}{B^2} \tag{1.6}$$

the formula for $\vec{E} \times \vec{B}$-drift. All we need then to run a model of space weather is start measurement of the plasma in the ionosphere and a model for the ongoing creation and loss of plasma in the ionosphere. Fortunately, both exists (Prölss and Bird, 2004). The space weather model is then free to forecast the flows. Thusly predicting where plasma densities is high and can produce problems for satellite communication.

1.3 Goal

In this thesis I wish to estimate the time variation of the nightside reconnection rate (Φ_N), so that it can be used in a space weather model. Available to me to do this, I have SW parameters and the open magnetic flux content of the polar caps. From that, I see three ways I could proceed: 1) I could attempt to produce a probabilistic function for Φ_N, based on a statistical study of Φ_N and my dataset. 2) I could somewhat foolhardy attempt to parametrize Φ_N using SW data. 3) Some sort of a combination of the two aforementioned points.

In the end I settled on point 2), as it is not out of the question that a function based on the solar wind can work as a time averaged function for Φ_N, since the previous studies seem to have focused more on instantaneous correlations. That coupled with the fact that 2) has a more straightforward method, which is needed considering the time constraint on this thesis, became the deciding factor. However, I still present my thoughts on a probabilistic function in section 4.3.

To parametrize Φ_N I set up several test parametrizations and do a analysis during times where F_{PC} is decreasing, I call these intervals flux closure events (FCEs); similarly I will call intervals when F_{PC} is growing polar cap expansion phases (PCEPs). When the best parametrization is found, I take it as a best guess and put it into a gradient-following algorithm to find the set of parameters that maximizes the correlation.

1.4 The Data

The data set used here consists of solar wind parameters from the OMNI data set and the calculated amount of magnetic flux within the polar cap. The data ranges from 01.01.10 00:05 UT to 23.06.17 23:55 UT, with time steps of 2 min. The OMNI solar wind parameters are measured by the MAGnetometer instrument(MAG), and the Solar Wind Electron, Proton, and Alpha Monitor (SWEPAM) onboard the The Advanced Composition Explorer spacecraft (ACE). ACE is located on the Earth-Sun line at Lagrange point 1 (or close too it). The data is then time-shifted to the location to of the Earth's bow shock nose.

Magnetic Flux

The amount of magnetic flux within the polar cap F_{PC} is determined through a multi-step process. It begins with data from the Active Magnetosphere and Planetary Electrodynamics Response Experiment (AMPERE). AMPERE takes magnetic perturbation data provided by the Iridium satellites and increases the time resolution by a factor of 10 to 20 s/sample during normal mode and by a factor of 100 in high-rate sampling when the resolution is increased to 2 s/sample. This allows the global radial current density to be estimated every 2 min, although the true update rate is 10 min commensurate with the inter-satellite time spacing in each orbit plane. (Clausen et al., 2012, 2013) The Iridium System consists of 66+ satellites in six polar orbits at 780km altitude. Onboard they have magnetometers measuring the magnetic field vectors across and parallel to the orbit, and the Earth centered radial component. From that the deviations $\Delta\vec{b}$ from the main magnetic field $\vec{B_0}$ can be found. These $\Delta\vec{b}$ are related to FAC through Ampere's law. This allows $\Delta\vec{b}$ to be expressed as a function of the gradient to a potential function. This current potential function is expanded using spherical harmonics. A least squares merit function is then used to find the current potential function that fits the measured $\Delta\vec{b}$ best. The global distribution of $\Delta\vec{b}$ can then be calculated, which in turn is used in Ampere's law to obtain the global FAC densities (Waters et al., 2001).

From the FAC densities Clausen et al. (2012) estimate the location of region 1 & 2 Birkeland currents. They fit the FACs at 24 MLTs, as a function of the magnetic latitude. The fit used is a product of a Gaussian and a one period sinusoidal. The Gaussian part simply pics out the area with the strongest currents, whilst the sinusoid adds the bipolar signature of the currents. This allows one to identify the location of region 1 Birkeland current as the poleward extrema of the fit (red vertical line in the right panel fig. 1.3), and the region 2 Birkeland current as the equatorward extrema. A truncated cosine function is then fitted to the location of region 1 Birkeland current at 24 local times, to get the full oval (left panel fig. 1.3).

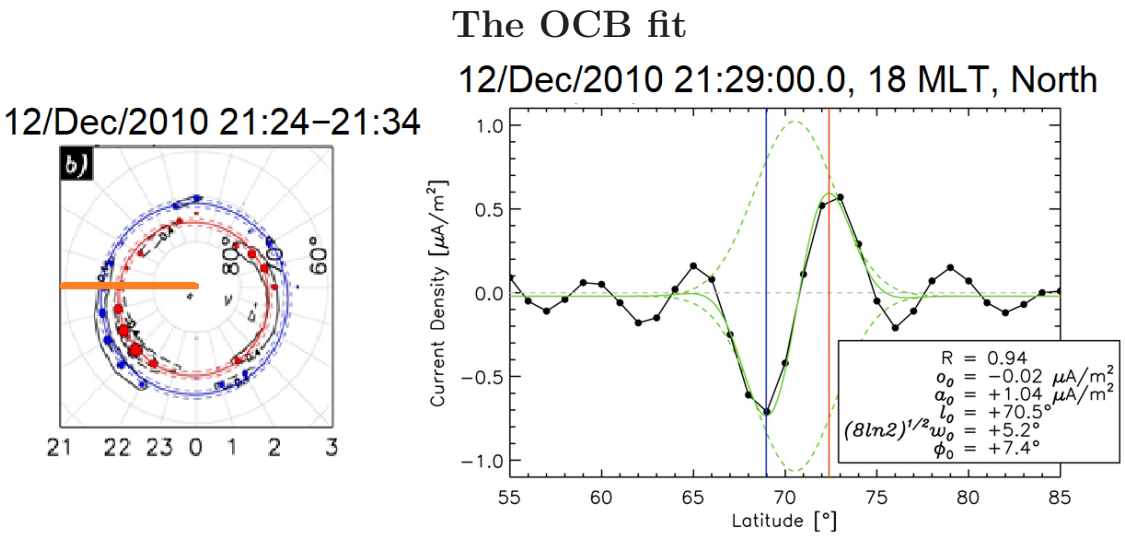

Figure 1.3: The right figure show how the OCB is fitted for a specific MLT. The left figure shows the OCB fit formed from the fits at different MLTs (dots), the size of FAC at the different MLT fits is indicated by the size of the dots. The thick line show 18:00 MLT, where the right figure is taken from (some minutes later). Adapted from Clausen et al. (2012)

The location of region 1 Birkeland currents is supposed to coincide with the OCB, and it is indeed found that it's statistically a good proxy for the OCB. This allows one to integrate the magnetic flux within the oval enclosed by the region 1 Birkeland currents, as a proxy for the amount of open magnetic flux in the polar cap (Clausen et al., 2013).

Dayside reconnection rate

Milan et al. (2012) found a parametrization of the dayside reconnection rate using solar wind parameters. To achieve this they identify 26 intervals where the polar cap expands while the nightside activity is low. They then set up a test parametrization based on the solar wind parameters. Where each parameter is raised to the power of some constant. These constants are then varied within a certain interval, which leaves many possible parametrizations for the dayside reconnection rate Φ_D of the following form:

$$\Phi_D = \Lambda N_p^{\alpha} v_X^{\beta} B_{YZ}^{\gamma} \sin^{\delta}(\frac{1}{2}\theta) \tag{1.7}$$

N_p is the number density, v_X the X-component of the solar wind speed, B_{YZ} the component of magnetic field in the YZ-plane in geocentric solar magnetospheric (GSM) coordinates, and θ the clock angle (shown in figure 1.4). α, β, γ and δ are the constants. Λ is a scale factor needed to adjust for the units of Φ_D.
For each configuration of the constants, they integrate over time to get the time variation of the flux within the polar cap.

$$F'_{PC}(t) = \int_{t_1}^{t2} \Phi_D(\alpha, \beta, \gamma, \delta, t)\, \mathrm{d}t \tag{1.8}$$

The calculated variation F'_{PC} is then compared with the observed variation in F_{PC}. The real amount of flux within the polar cap was in their case obtained from auroral images, taken by the Far Ultraviolet (FUV) instrument onboard the Imager for Magnetopause-to- Aurora Exploration (IMAGE) spacecraft. To determine the best fit between the observed flux and the calculated flux, they calculate the Pearson Correlation Coefficient (PCC), see Appendix A. The scale factor Λ is decided by comparing the size of integral of the best fit with the measured open flux. This is done after the PCC is calculated, as scaling the fit and/or adding a constant does not affect the PCC. After the fitting process it is found that $\alpha = 0$, i.e. the dayside reconnection rate is independent of the number density. In the end they find that the following parametrization is a good description of Φ_D.

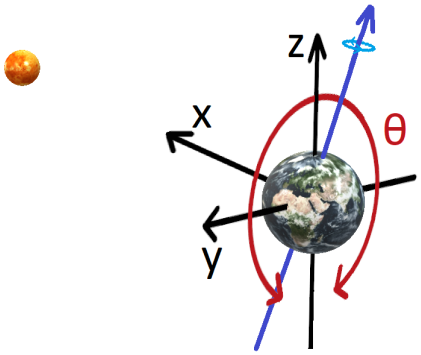

Figure 1.4: Clock Angle in GSM coordinates, The X axis points towards the Sun and its Z axis is the projection of the Earth's magnetic dipole axis (positive North) on to the plane perpendicular to the X axis, and the Y is given by the right hand rule. Earths rotational axis is shown in blue.

$$\Phi_D = \Lambda v_X^{4/3} B_{YZ} \sin^{9/2}(\frac{1}{2}\theta) \tag{1.9}$$

Where Λ is $3.3 \times 10^5 \mathrm{m}^{2/3}\mathrm{s}^{1/3}$, the unit $\mathrm{m}^{2/3}\mathrm{s}^{1/3}$ is needed to give Φ_D the unit Volt. This parametrization achieves a PCC value of 0.972 (where 1 is max).

Gaps in the data

With data spanning 7.5 years at a so high resolution, it should not come as a surprise that there are some gaps in the data. There are three possible reasons that give a data gap. These are: 1) If for some reason OMNI data is missing; 2) If data from AMPERE are unavailable; 3) If the FACs found by AMPERE are too weak to reliably determine the location of the Birkeland currents. 1) and 2) are somewhat self-explanatory, 3) however needs some elaboration.
Accurately determining the location of the OCB is extremely important to calculate F_{PC}. Say for example that the true OCB location is at 75° MLAT whilst the approximation says 73° MLAT, the difference between the true F_{PC} and found F_{PC} would be around 30%. So knowing how reliable the OCB fit is, is important. When fitting for data between January 2010 and August 2011, Clausen et al. (2012) found that for 5% of the available AMPERE data the method is not able to fit for a sufficient number of MLT to determine the oval. When it comes to the successful fits for the OCB, they found that the uncertainty of the fit is large when the median current density of the successfully fitted locations is less than $0.2\mu\mathrm{A/m}^2$. Above $0.2\mu\mathrm{A/m}^2$ the uncertainty is found to be small and close to constant. So to ensure good data the method rejects times where the median current density is below the threshold of $0.2\mu\mathrm{A/m}^2$.

CHAPTER 2

Method

The method of determining a parametrization of Φ_N closely follows the method presented by Milan et al. (2012). In that, I have attempted to parameterize the nightside reconnection rate by the IMF parameters in much the same way. As Milan et al. (2012), I calculate the Pearson correlation coefficient (PCC). For each FCE I calculate $F_{PC}(t) - \langle F_{PC}(t) \rangle$ and $F'_{pc}(t) - \langle F'_{pc}(t) \rangle$, where the "observed value" F_{PC} is the time smoothed average of open magnetic flux in the northern hemisphere and the southern hemisphere. F'_{pc} is the integral of my attempted parametrization. The mean values ($\langle F_{PC}(t) \rangle$ and $\langle F'_{pc}(t) \rangle$) for each FCE interval are subtracted since I am interested in the change of magnetic flux not the absolute value. All the FCEs are then pooled together, and the correlation between the two series is calculated. Shortly said the PCC value gives a measurement of how good the parametrization is. This thesis relies so heavily upon the PCC that I give it its own introduction in Appendix A.

As a starting point I have taken the same parametrization as Milan et al. (2012) and aim to find the exponents anew for Φ_N. The thought being that since the amount of flux put into the polar cap is described by such a function, the amount leaving the polar cap may be so as well. As we know, the polar cap neither expands nor contracts indefinitely, so that which goes in must come out. However, we do expect different values for the exponents as the IMF changes between the PCEP and FCE onset, and FCEs will in general have a different duration and intensity. Even though Φ_D is independent of solar wind density N_p, that is not necessary the case for Φ_N. Therefore N_p will be included in my attempts. I also have the solar wind dynamic pressure p_d available to me, but I choose not to use it. As the dynamic pressure is a function of the density and wind speed, and some constant will not affect the fitting process, any dependency on the dynamic pressure will manifest in the exponents of v_T and N_p.

For the Φ_D found by Milan et al. (2012) B_{YZ} is the configuration of the IMF that gives the best result. That can however not be assumed to be the correct choice for Φ_N, since the magnetotail presents a different surface to the IMF than the closed magnetic field on the dayside. So I test four different configurations for the IMF; B_{YZ}, B_{Tot}, B_{XY} and B_{XZ}. Whether the Φ_N should have a maximum for southward IMF or northward IMF is also uncertain. Therefore, both $\Theta = \theta$ and $\Theta = \pi - \theta$ are tested.

I then have eight parametrizations of the following form:

$$\Phi_N = \Lambda B^{\alpha} v_T^{\beta} N_p^{\delta} \sin^{\gamma}(\frac{1}{2}\Theta) \tag{2.1}$$

where $\alpha, \beta, \gamma, \delta$ are the exponents I want to determine. However, there is one problem that remains. All of the IMF parameters are given at the bow shock. Although this is fine for dayside reconnection which happens at the magnetopause, close to the bow shock, it not necessarily so for the nightside reconnection. So as a final thing before I start the fitting process I allow for a time shift in the IMF data, so that the time delay from the IMF arrival at the bow shock until the effect on the FCE starts may be accounted for.

The IMF time shift

I think of the time shift as a travel time from the bow shock to a place k where IMF parameters interact with the magnetosphere to create the FCEs in some way. So instead of finding the time shift t_0 directly, I find the average location where the IMF interacts with magnetosphere. To do this I firstly say that the bow shock nose at all times located at $15R_E$ from Earth, as this is an often used general location for the bow shock nose (Petrinec, 2002). I then add k to the correlation process as a free parameter.
For every parametrization I test, I also time shift the IMF parameters to multiple locations k and calculate the PCC. To do the time shift for a given data point, I find the data point that has moved closest to the specified location k. This is done by calculating the average solar wind speed using the last 25 measurements. I then find the location of the last 25 data points using this average speed. This averaging is done to keep the data points from passing one another. The measurement point closest to the test location is then chosen. Yielding the effective time shift as the time difference between the chosen point and the current time.

The scale factor Λ

The PCC is independent of the scaling such that Λ is free to be determined at any time. That is done by finding the Λ that minimizes the difference between the series for F_{PC} and F'_{pc}

$$Diff = \sum |F_{PC} - F'_{pc}| \tag{2.2}$$

To save time, this is only done for the parametrization that gives the best PCC.

There is however a possibility that Λ is not a constant, but rather a function of something. One possibility is that it is a function of F_{PC} in some way. This can make sense since Φ_N often is stronger for high values of F_{PC}. To test this I let $\Lambda = \lambda F_{PC}(t - t_1)$. Here a time shift t_1 is added, to see if it can help give Φ_N the correct form. Since $\Lambda = \lambda F_{PC}(t - t_1)$ is not a equal scaling for every data point it will affect the PCC. I therefore have eight new parametrizations to test. Since I am not interested in the size of F_{PC}, but rather the time development in it, is a scaled (to Gigaweber) version used.

$$\Phi_N = \lambda F_{PC}(t - t_1) B^{\alpha} v_T^{\beta} N_p^{\delta} \sin^{\gamma}(\frac{1}{2}\Theta), \tag{2.3}$$

bringing the total up to 16 parametrizations.

The correlation

The actual correlation is done in three steps:
1) α, β, δ are varied with a step length of 0.5 between -2 and 2. γ is varied with the same step length but between 0 and 6. The time shift for the IMF data is given some locations k between $15R_E$ and $-15R_E$, whilst the time shift t_1 for F_{PC} (when that is used) is given some test values between 0min and 30min. This gives a grid of PCC values for each attempted parametrization. The parameters that gives the best PCC, is then chosen for each parametrization and sent to the next step. 2) In the hope that values from the last step is the closest point to a global maximum for the PCC value, an iterative gradient-following is started in that point. That will then hopefully find the global maximum for the PCC. For this algorithm the boundary values for $\alpha, \beta, \gamma, \delta, t_1$ remain the same, but k is now allowed to be anywhere between $15R_E$ and $-250R_E$. 3) Finally I take the best result of the 16 parametrizations, and calculate contour plots of the parameter space around the solution. This gives an idea whether the solution has reached a global maximum, or just a local one. This method proceeds the same way for both Method 1 and Method 2, see below.

The two Methods

There are two alternatives for how to perform the correlation. Similarly to Milan et al. (2012) who assumes the nightside reconnection to be zero during growth phases, I can assume that the dayside reconnection is zero during the FCEs. The integration to get F'_{pc} will be:

$$\frac{\mathrm{d}F'_{pc}}{\mathrm{d}t} = -\Phi^*_N \tag{2.4}$$

This will give the net-flux closure rate Φ^*_N, regardless of whether the assumption is correct or not. If the assumption holds true, it will equal the nightside reconnection rate. If not then the dayside reconnection rate can be added to get the full nightside reconnection rate.

The alternative method is to include Φ_D determined from Milan et al. (2012) and use eq. 1.2:

$$\frac{\mathrm{d}F'_{pc}}{\mathrm{d}t} = \Phi_D - \Phi_N \tag{2.5}$$

Using eq. 2.4 will be referred to as Method 1 and eq. 2.5 as Method 2. Both these methods have weaknesses and strengths, which are discussed in section 4.2.

Method 2 requires Φ_N to be properly scaled before the correlation process, as subtracting it from Φ_D is not a linear process. So to do that $\frac{\mathrm{d}F_{PC}}{\mathrm{d}t}$ is calculated and put into eq. 2.5 to find the "observed" nightside reconnection rate $\Phi_{N_{obs}}$, from that the constant part of the scale factor can be estimated as $\lambda = \langle\Phi_{N_{obs}}\rangle / \langle\Phi_N\rangle$. This is not a rigorous way to do this, but it is considerable faster than using equation 2.2 to find the best scale factor.

Identifying the FCEs, and limiting the data set

I identify FCEs as times where $\frac{\mathrm{d}F_{PC}}{\mathrm{d}t}$ is negative. To mitigate adverse effects from gaps in the data are FCEs containing gaps of 15 min and more split into separate FCEs at those points. Since the prehistory of F_{PC} is not of interest here, F'_{pc} is set to be equal to F_{PC} at the start of every FCE. Therefore a certain length of the FCEs required to see the development in F'_{pc}. I therefore only keep FCEs containing 4 data points or more.

This correlation takes a fair time to run, so I am forced to limit the data set. I use data from the period 01/04/15-11/07/15, this interval was chosen because problem with gaps in data and badly behaved Φ_D (discussed later) seemed to be small there. In this interval, I find 2154 FCEs that fulfil my demands, averaging a length of 8 data points.

CHAPTER 3

Results

3.1 General Observations

Before I jump into the results for the two methods, it is important to look at the data and the way it is processed. That can tell whether results are useful or not. Firstly, F_{PC} needs to be determined. Figure 3.1 shows the mean amount of open flux in the two polar caps compared with the amount in each polar cap (NFlu - north, SFlu - south). From that we can see that variation in NFlu and SFlu compared with the mean is at times large. Worst seems to be times where the mean is large, like 02:00UT - 06:00UT. Also, interestingly there seem to be periods where one of the polar caps is consistently larger than the other.

The mean is clearly badly behaved at certain times, as seen by the spikes in figure 3.2. It is for example highly unlikely that the mean should be able to increase with 0.4 GWb in 2 min and the immediately decrease with 0.4 GWb during the next 2 min as seen 20:00 UT. So to smooth out those badly behaved times I use an average over 9 data points, assuming equally spaced points corresponds to a 16 min interval, to get F_{PC}. As seen from figure 3.2 it is much better behaved. However, there are areas where it does not reach the extrema it should, like 02:00 UT and 07:00 UT where it does not go as low as it should; or around 09:00 UT where it do not goes as high as it should.

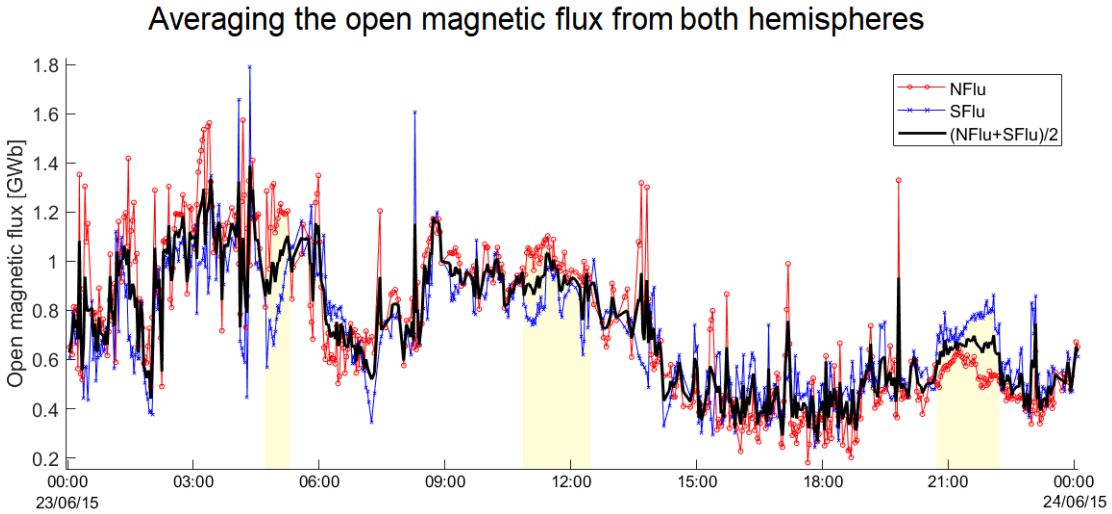

Figure 3.1: The result of averaging the open magnetic flux in the northern polar cap $NFlu$ and the southern polar cap $SFlu$, for 23.06.15. Shaded areas show intervals where $NFlu$ and $SFlu$ is notably different.

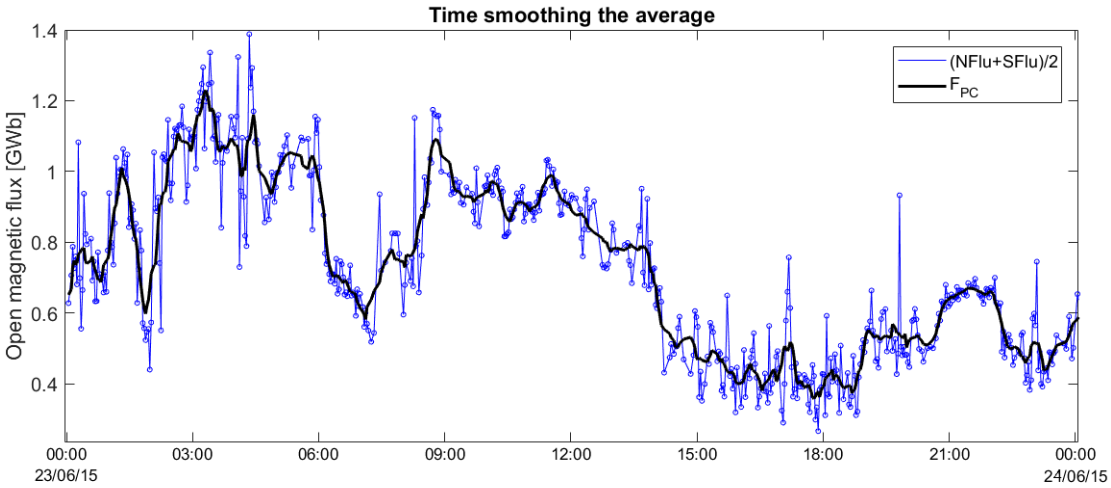

Figure 3.2: The time smoothed average magnetic flux within the polar caps, for the 23.06.15.

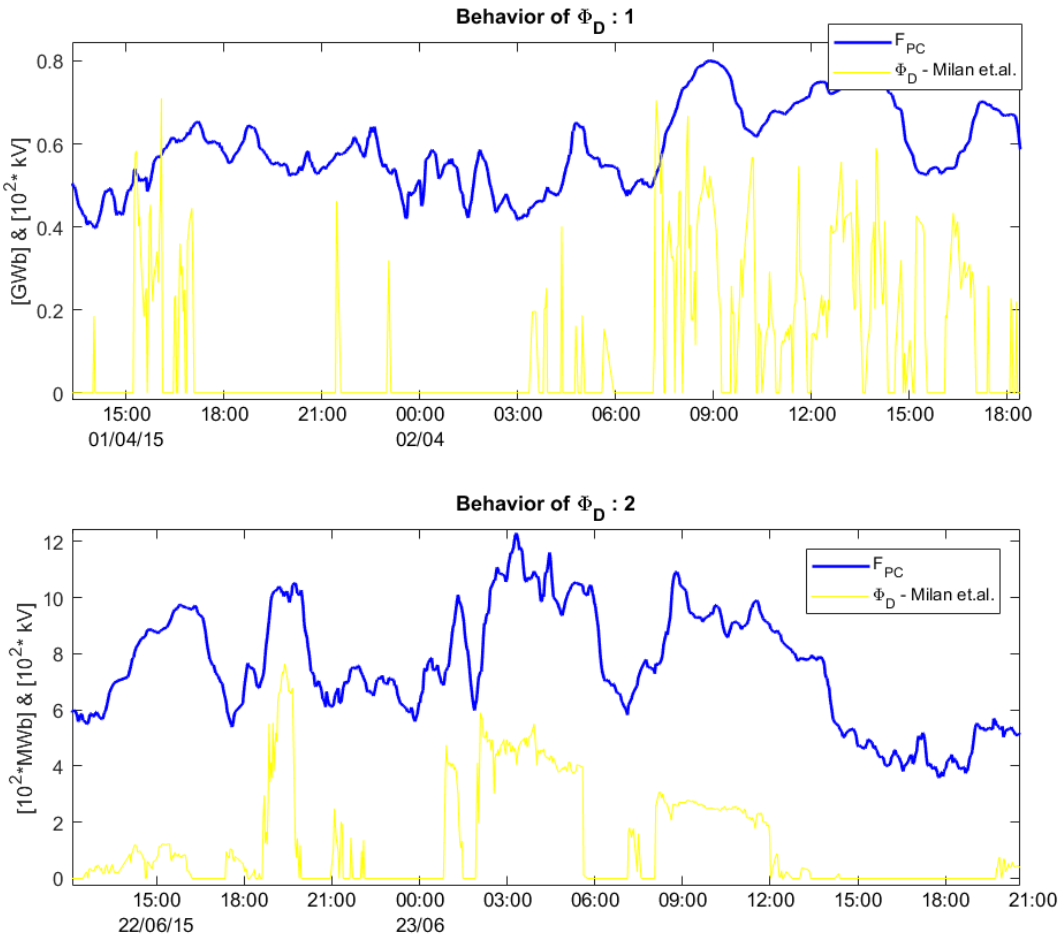

Figure 3.3: Comparison of the dayside reconnection (Milan et al., 2012) and F_{PC}. Top panel 01-02/04/15, shows PCEPs not accounted for by Φ_D. Bottom panel 22-23/06/15, shows periods with suspiciously high reconnection rates.

In calculating the dayside merging rate given by Milan et al. (2012), there is the question: whether it is valid for northward pointing IMF or not. In this I have followed Clausen et al. (2013) and put $\Phi_D = 0$ when $Bz > 0$. Either way, Φ_D would be very small for northward IMF, as the function is sharply dependent on the clock angle. With a small or zero dayside reconnection rate like it often is during northward IMF, is F_{PC} not expected to grow. However, that is clearly not the case as seen in the top panel in figure 3.3, where F_{PC} still grows during those times. If not put to zero, Φ_D is still way too small to produce the observed changes.
On the opposite end of the spectrum the question becomes how large Φ_D is allowed to get. In the bottom panel of figure 3.3. we can see some interval where Φ_D gets very large, reaching a maximum of 764 kV. In comparison the largest values Milan et al. (2012) present is around 300 kV. Since I do not know what to do with Φ_D, I am forced to keep it as is.

3.2 Results Method 1

Results Method 1, without $\boldsymbol{F_{PC}}$

Argument of the sine:	θ				$\pi - \theta$			
B-field component:	B_{YZ}	B_{Tot}	B_{XY}	B_{XZ}	B_{YZ}	B_{Tot}	B_{XY}	B_{XZ}
α	0.348	0.458	0.266	0.273	0.340	0.455	0.242	0.255
β	0.875	0.737	0.806	0.783	0.832	0.676	0.796	0.755
γ	0	0	0	0	0.127	0.165	0.170	0.188
δ	0.005	-0.025	0.046	0.042	-0.022	-0.075	0.040	0.035
$k[R_E]$	-5.58	-9.22	14.98	-14.87	-2.58	-9.16	13.03	-9.27
PCC	0.883	0.880	0.871	0.873	0.885	0.882	0.873	0.876

Table 3.1: The highest correlations between $F_{PC}(t) - \langle F_{PC}(t)\rangle$ and $F'_{pc}(t) - \langle F'_{pc}(t)\rangle$ during FCEs, for the eight configurations of B and Θ in $\Phi^*_N \approx dF'_{pc}/dt = B^\alpha v_T^\beta N_p^\delta \sin^\gamma(\frac{1}{2}\Theta)$. All the IMF parameters are time shifted to $k \cdot R_E$, where $k = 15$ is the assumed location of the bow shock nose and $k = 0$ is at Earth and so on.

Results Method 1, with $\boldsymbol{F_{PC}}$

Argument of the sine:	Θ=θ				Θ=$\pi - \theta$			
B-field component:	B_{YZ}	B_{Tot}	B_{XY}	B_{XZ}	B_{YZ}	B_{Tot}	B_{XY}	B_{XZ}
α	0.304	0.356	0.219	0.201	0.295	0.338	0.149	0.213
β	0.473	0.372	0.416	0.490	0.420	0.295	0.390	0.310
γ	0	0	0	0	0.314	0.323	0.352	0.351
δ	-0.083	-0.091	-0.046	-0.016	-0.121	-0.126	-0.052	-0.082
$k[R_E]$	15.00	14.94	15.00	-16.00	-1.93	-1.82	-1.82	-8.27
t_1[min]	18.6	20.0	22.3	19.9	22.4	23.0	20.4	22.1
PCC	0.887	0.883	0.877	0.877	0.896	0.892	0.887	0.888

Table 3.2: The highest correlations between $F_{PC}(t) - \langle F_{PC}(t)\rangle$ and $F'_{pc}(t) - \langle F'_{pc}(t)\rangle$ during FCEs, for the eight configurations of B and Θ in $\Phi^*_N \approx dF'_{pc}/dt = F_{PC}(t - t_1)B^\alpha v_T^\beta N_p^\delta \sin^\gamma(\frac{1}{2}\Theta)$. All the IMF parameters are time shifted to $k \cdot R_E$, where $k = 15$ is the assumed location of the bow shock nose and $k = 0$ is at Earth and so on. The best result for Method 1 is highlighted.

Using equation 2.4 to describe the change in F_{PC} during FCEs the correlation analysis yields the results presented in table 3.1 and table 3.2, after the first two steps in the fitting process. Each column shows the best result for a configuration of Θ and B-component. The exponents $\alpha, \beta, \gamma, \delta$ and the PCC value are rounded to three significant digits, as smaller changes does not have much of an impact. By the same argument is k rounded to two decimal points and t_1 to one, which probably is higher than needed.

From the tables we can see that the PCC value is consistently higher for the reverse clock angle, meaning a maximum in the nightside reconnection for northward IMF is preferable, whilst attempts of using the clock angle ends up being independent of the sine, and thusly yields a lower PCC value. The best choice of IMF component is consistently found to be B_{YZ}, as with the dayside reconnection. Lastly the inclusion of F_{PC} with a time delay increases the PCC for all the configurations of Θ and B. The best parametrization is then:

$$\Phi_N^* = \lambda F_{PC}(t - 22.4\text{min}) B_{YZ}^{0.295} v_T^{0.420} N_p^{-0.121} \sin^{0.314}\left(\frac{1}{2}(\pi - \theta)\right) \tag{3.1}$$

with the IMF parameters time shifted to -1.93R_E.

The time shifts for the IMF parameters do not seem to be particularly stable. The location used in the parametrization of the IMF time shift varies from ca. 15R_E to -16R_E. The time shift for F_{PC} is on the other hand far more stable, only varying between 18 and 23 min. Since the time shifts should be the same for all the parametrizations it indicates that the correlation varies little with the time shifts, or that it has many local maxima and my fitting has found a wrong maximum for several of the parametrizations. Looking at the bottom panel figure 3.4, which is the time shift parameter space for the best fit, the "flat" nature indicates that determination of $\alpha, \beta, \gamma, \delta$ is the dominating factor in the PCC evaluation. Whilst changes in the time shift in comparison modifies the PCC very little. From figure 3.4 we can see that the fitting process has found what appears too be a global maxima for the PCC value. Based on figure 3.4 I change the time shifts too $t_1 = 20$ min and $k = -1.5\text{R}_\text{E}$, as that gives a marginally better fit.

The scale factor is then found to be $\lambda = 7.018 \cdot 10^5$ (with the appropriate units to give Φ_N the unit Volt) by minimizing $Diff$ in equation 2.2. The best result using Method 1 is then:

$$\Phi_N^* = 7.018 \cdot 10^5 \cdot F_{PC}(t - 22.0\text{min}) B_{YZ}^{0.295} v_T^{0.420} N_p^{-0.121} \sin^{0.314}\left(\frac{1}{2}(\pi - \theta)\right), \tag{3.2}$$

with the IMF parameters time shifted to $k = -1.5\text{R}_\text{E}$.

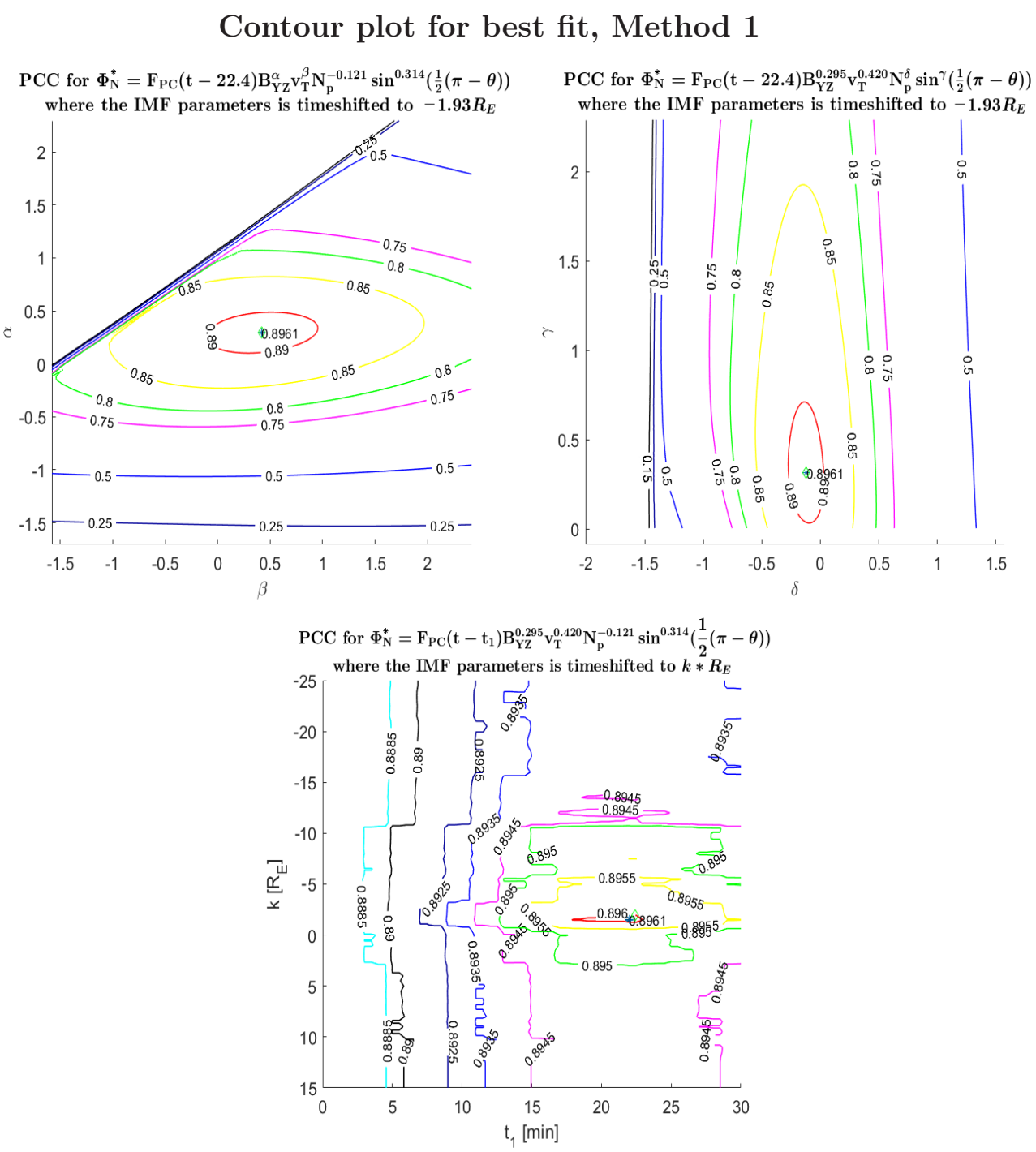

Figure 3.4: Contour plots of the parameter space around the best fit for Method 1.
The three panels show different slices of the parameter space, upper left the exponents for the B_{YZ} and v_T - α and β, upper right the exponents for the sine and N_p - γ and δ, bottom panel the time shift space for IMF parameters and F_{PC} - k and t_1. Diamond marks the best fit found after the first two steps. The asterisk shows the best PCC value in the grid used in the plot.

3.3 Results Method 2

Results Method 2, without $\boldsymbol{F_{PC}}$

Argument of the sine:	θ				$\pi - \theta$			
B-field component:	B_{YZ}	B_{Tot}	B_{XY}	B_{XZ}	B_{YZ}	B_{Tot}	B_{XY}	B_{XZ}
α	0.640	0.777	0.460	0.639	0.634	0.783	0.481	0.605
β	1.154	0.974	1.144	0.994	1.113	0.938	1.105	0.961
γ	0.628	0.571	0.548	0.474	0	0	0	0
δ	-0.085	-0.117	0.011	-0.047	-0.140	-0.166	-0.020	-0.069
$k[R_E]$	14.98	14.98	15.00	-13.99	14.99	14.98	14.99	-25.93
PCC	0.839	0.826	0.780	0.810	0.809	0.800	0.766	0.782

Table 3.3: The highest correlations between $F_{PC}(t) - \langle F_{PC}(t)\rangle$ and $F'_{pc}(t) - \langle F'_{pc}(t)\rangle$ during FCEs, for the eight configurations of B and Θ in $\Phi_N = B^{\alpha} v_T^{\beta} N_p^{\delta} \sin^{\gamma}(\frac{1}{2}\Theta)$. All the IMF parameters is time shifted to $k \cdot R_E$, where $k = 15$ is the assumed location of the bow shock nose and $k = 0$ is at Earth and so on.

Results Method 2, with $\boldsymbol{F_{PC}}$

Argument of the sine:	θ				$\pi - \theta$			
B-field component:	B_{YZ}	B_{Tot}	B_{XY}	B_{XZ}	B_{YZ}	B_{Tot}	B_{XY}	B_{XZ}
α	0.520	0.614	0.372	0.493	0.511	0.642	0.388	0.462
β	0.712	0.544	0.647	0.548	0.638	0.495	0.581	0.562
γ	0.302	0.269	0.234	0.237	0	0	0	0
δ	-0.159	-0.174	-0.099	-0.118	-0.192	-0.202	-0.121	-0.132
$k[R_E]$	15.00	14.67	14.73	-6.58	14.93	-11.83	14.90	-17.79
t_1[min]	24.2	18.4	18.7	22.0	18.5	21.8	19.0	18.9
PCC	0.870	0.856	0.822	0.841	0.861	0.847	0.818	0.833

Table 3.4: The highest correlations between $F_{PC}(t) - \langle F_{PC}(t)\rangle$ and $F'_{pc}(t) - \langle F'_{pc}(t)\rangle$ during FCEs, for the eight configurations of B and Θ in $\Phi_N = F_{PC}(t - t_1) B^{\alpha} v_T^{\beta} N_p^{\delta} \sin^{\gamma}(\frac{1}{2}\Theta)$. All the IMF parameters is time shifted to $k \cdot R_E$, where $k = 15$ is the assumed location of the bow shock nose and $k = 0$ is at Earth and so on.

Using equation 2.5 to describe the change in F_{PC} during FCEs yields the results shown in table 3.3 and table 3.4, after the first two steps in the fitting process. Again one can see that B_{YZ} is the best choice of B-component, and that adding F_{PC} increases the PCC. The big change from Method 1 is in the choice of the angle Θ. Now the function becomes independent of the sine for parametrizations with a maximum for northward IMF. For a maximum during southward IMF the parametrizations chose a low dependency on the sine, giving better PCC values than the northward counterparts. The best parametrization found is now:

$$\Phi_N = \lambda F_{PC}(t - 24.2\text{min}) B_{YZ}^{0.520} v_T^{0.712} N_p^{-0.159} \sin^{0.302}\left(\frac{1}{2}\theta\right) \tag{3.3}$$

using IMF parameters at the bow shock nose.

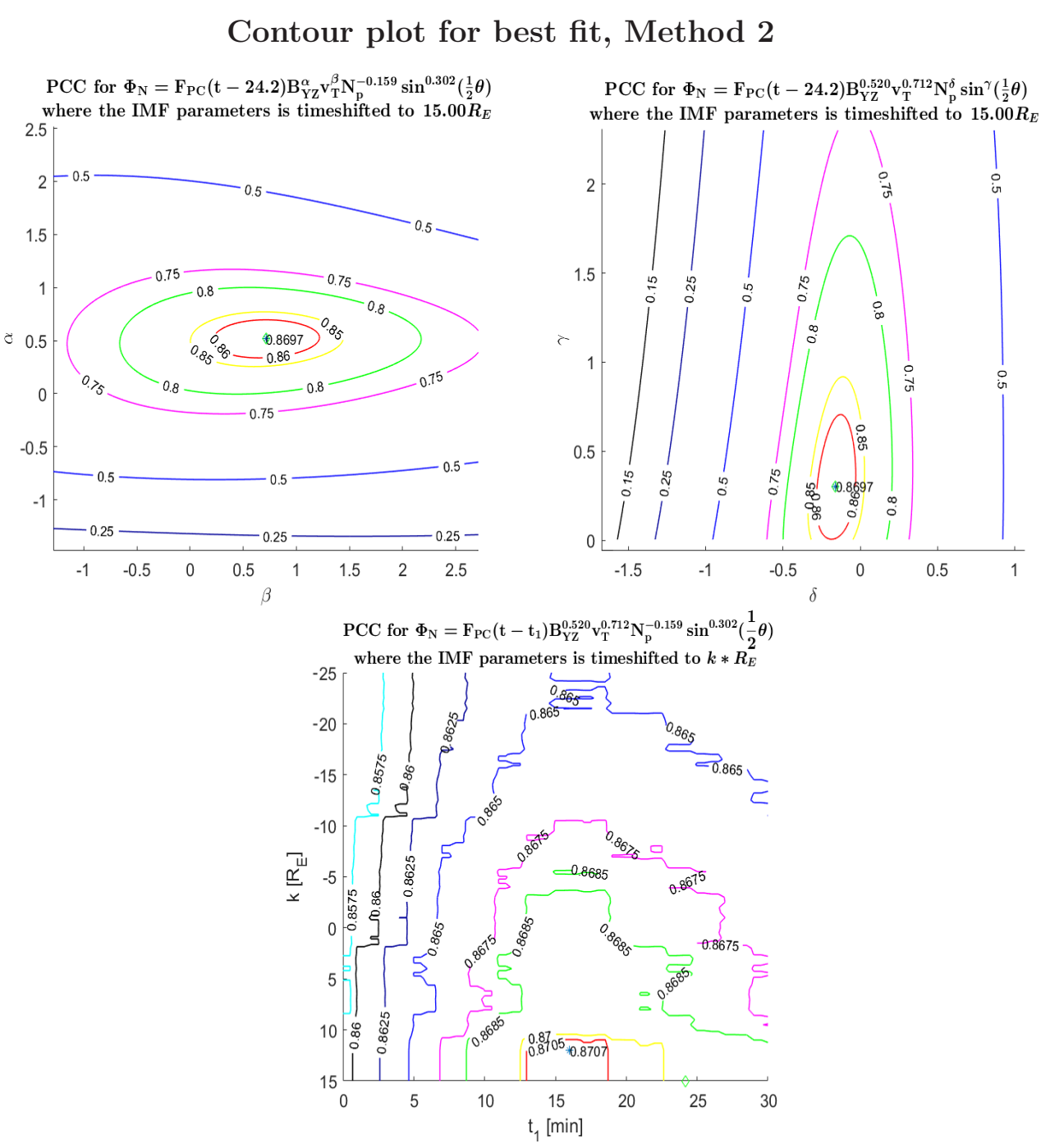

Figure 3.5: Contour plot of the parameter space around the best fit for Method 2.
The three panels show different slices of the parameter space, upper left the exponents for the B_{YZ} and v_T - α and β, upper right the exponents for the sine and N_p - γ and δ, bottom panel the time shift space for IMF parameters and F_{PC} - k and t_1. Diamond marks the best fit found after the first two steps. The asterisk shows the best PCC value in the grid used in the plot.

From figure 3.5 we can see that also this parametrization has found what appears too be a global maximum in $\alpha, \beta, \gamma, \delta$ space. And again is the time shift space very "flat", not impacting the PCC as much as $\alpha, \beta, \gamma, \delta$. Looking at the time shift-space (bottom panel figure 3.5) makes me think that the gradient following algorithm must have ended up in a local maximum. So I choose to use $t_1 = 16$ min and $12.00\mathrm{R_E}$, as that is the best point in the grid used to plot the contours, and its placement suggest that it can be global maximum.
For this method, the scale factor has an effect on the PCC so an estimate is used in correlation. That estimate is for the best fit (eq. 3.4) $2.214 \cdot 10^6$, but using equation 2.2 the scale factor is found to be $2.639 \cdot 10^6$. That new scale factor boosts the PCC for the best fit to 0.878, yielding the final parametrization for Method 2 as:

$$\Phi_N = 2.639 \cdot 10^6 \cdot F_{PC}(t - 16.0\mathrm{min}) B_{YZ}^{0.520} v_T^{0.712} N_p^{-0.159} \sin^{0.302}\left(\frac{1}{2}\theta\right), \tag{3.4}$$

with the IMF parameters only slightly time shifted inwards, to $k = 12\mathrm{R_E}$.

3.4 Comparisons

Figure 3.6 shows F_{PC} from 06:00 UT 27/04/15 to 18:00 UT 28/04/15, and F'_{pc} estimated using Method 1 (red asterisks) an using Method 2 (purple diamond) during the FCEs. For FCE, staring 07:40 UT the 27/04, neither method is able to follow the sharp drop in F_{PC}. The next FCE is cut short because of a long gap in the data, but it can be seen that both methods still underestimate Φ_N. For the rest of FCEs both methods estimate F_{PC} much better, with the exception of the FCE starting just before midnight 28/04, so what is the difference between the FCEs, where they preform badly and the rest? Investigating IMF parameters for this interval I find that v_T, B_{YZ} and Θ is of comparative sizes during this entire 2 day interval. N_p is on the other hand notability larger during the FCEs where my Φ_N's cannot keep up. Values of N_p in these FCEs are $13 - 17$ cm^{-3} and in the rest of the interval $5 - 9$ cm^{-3}.

Lets also take a closer look at one of the FCE where both methods at first glance seems to do well. The zoomed-in box shows the start of the FCE beginning at 13:45 UT on the 28/04. Here we see two types of behavior that ideally should not be there. 1) It is actually two separate FCE, with the start of the second FCE interval being indicated by an arrow. The FCE is split in two since the derivative of F_{PC} is positive in a single point, causing the fits to jump back to the same value as F_{PC} and artificially driving the PCC value up. 2) As seen throughout the zoomed in window the data points are not equally spaced in time. Missing data points can be found throughout the interval. This causes the correlation to prefer fits that behave as an average over the time gap to the next point, instead of the average of 2 min, which the data is supposed to be spaced with. So to minimize this problem FCEs are divided at large gaps in the data, like seen for the third FCE in figure 3.6, if a gap exceeds 15 min.

Finally there is the question: how good are these methods combined with Φ_D at predicting F_{PC}? Sadly these functions do not approach zero when the polar cap expands, which is in conflict with Φ_D as it is found assuming Φ_N to be zero at those times. So just using equation 1.2 indiscriminately with the nightside reconnection rates found here will not work. In other words, there needs to be some sort of trigger for the beginning and end of FCEs. Assuming that such a trigger can be found and implemented, I get the result shown in figure 3.7, which shows how the open magnetic flux is estimated over a day by the different methods. To get an as relevant comparison as possible I have chosen a day where Φ_D seems to be well behaved. For this comparison Φ_N is set to zero during PCEPs, identified as times where $\frac{\mathrm{d}F_{PC}}{\mathrm{d}t} > 0$, in accordance with Milan et al. (2012). Method 1 & 2 are only implemented during the FCEs. Just to see how it does I have also taken the Φ_N found by Method 1 and put it into 1.2 during FCEs, I call this Method 1.1.

Figure 3.7 clearly shows that Method 1.1 ends up overestimating F_{PC} for most of the interval. This is not surprising as Method 1 in itself just estimates the net-closure rate, so adding Φ_D would cause it to underestimate the decreases F_{PC} or even have F'_{pc} growing during FCEs. Furthermore is Method 1 only really valid during FCEs, as it just estimates the net-closure rate and that would be negative during PCEPs, something the found function cannot be. Method 1 & 2 seem to behave quite well, seemingly having more problems with Φ_D than Φ_N. Towards the end of the interval is the calculated Φ_D so small that F'_{pc} never recovers from the FCEs and becomes negative. To say something more about FCEs in particular, table 3.5 shows the net sum of flux closure for the methods and F_{PC} during the FCEs shown in figure 3.7.

Table 3.5 show the net amount of closed flux during the FCEs shown in figure 3.7. This shows that Method 2 is the best at estimating the net amount of closed flux during most of the FCEs. Method 1.1 is the best for two FCEs, but this is mostly because Method 1 & 2 grossly overestimates, at those times. Otherwise Method 1 would be the best during those two FCEs, putting Method 1 & 2 close two being equally good. This can also be seen in figure 3.7, where they follow each other closely. Therefore, it is hard to say whether one is particularly better than the other.

Comparing the net amount of closed flux during FCEs 18/10/15

Time intervals	01:15-02:59	05:49-06:53	08:13-08:39	09:39-11:05	12:13-13:53	14:47-16:03	17:19-19:55
F_{PC}	294.7	270.4	56.0	522.8	166.4	187.2	339.9
Method 1	347.7	241.8	67.2	444.6	366.0	197.7	284.7
Method 1.1	293.4	202.6	−97.3	419.5	250.1	119.5	198.4
Method 2	349.8	247.0	22.9	484.4	397.1	197.2	296.7

Table 3.5: The net amount of flux closed during FCE intervals the 18/10/15. Shaded cells are the result closest to the amount observed in F_{PC}. All values are given in MWb.

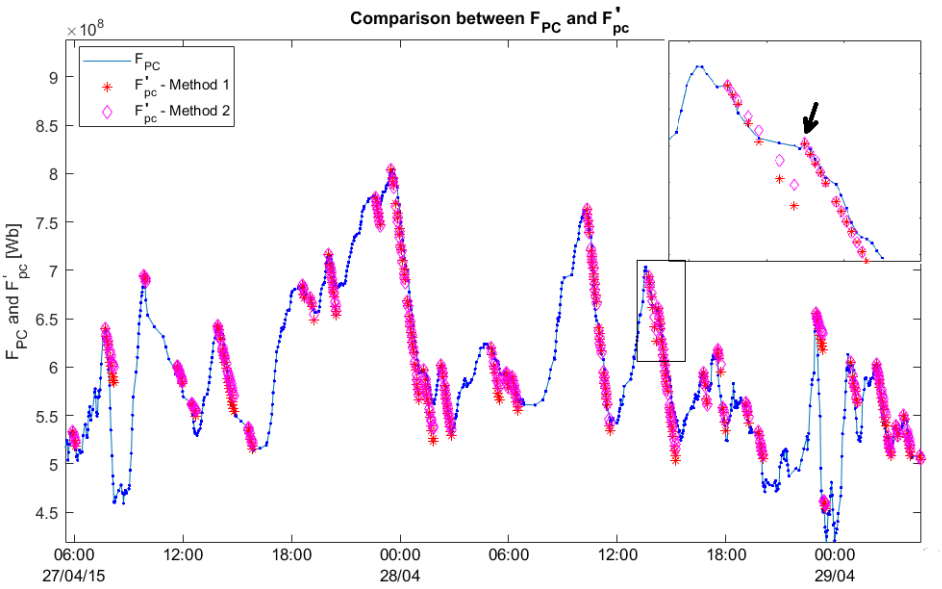

Figure 3.6: Comparison of F_{PC} and F'_{pc} during FCEs 27-28/04/15. Including a zoom on the FCE beginning at 13:45 UT the 28/04.

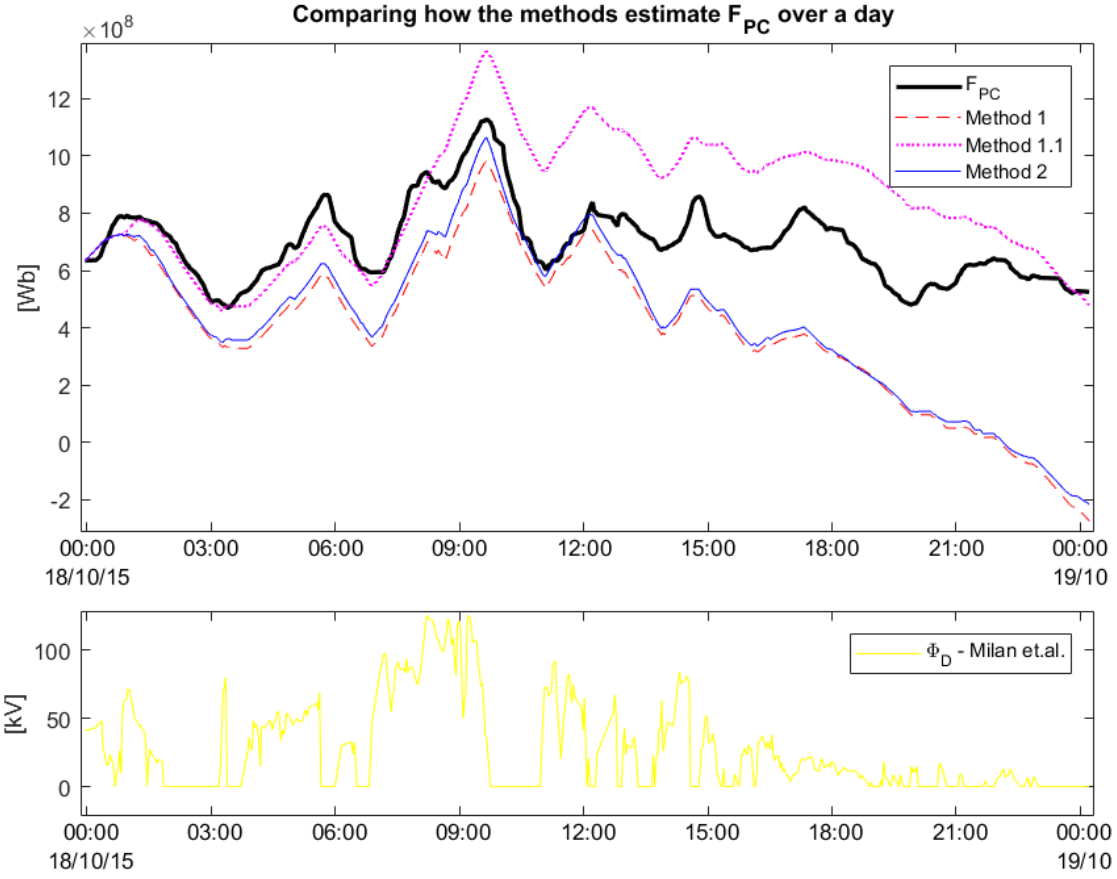

Figure 3.7: Testing whether Method 1 and Method 2 together with Φ_D (Milan et al., 2012), can accurately predict F_{PC}. Also included is Method 1.1 where Φ_N found by Method 1 is inserted in equation 1.2.

CHAPTER 4

Discussion

4.1 The data: multiple problems

The open magnetic flux

The size

To understand the results one must also understand the strengths and weaknesses of the data used. This is especially important for F_{PC} as it is the backbone of the correlation. The raw data used to obtain F_{PC} is processed through many layers. My focus now will be on the determination of the OCB location from the FAC data, as I have to assume the FAC data from AMPERE is correct. From Clausen et al. (2012) it is known that the region 1 Birkeland currents need to be of a certain size to produce accurate results in the determination of the OCB. Further is it shown by Clausen et al. (2013) that the determination of the OCB is good during substorm intervals. The FCEs that I look at do not necessarily correspond to substorms. Therefore I need to say something about the quality of F_{PC} throughout the data set, however I do not have FAC data so I must use the determination itself and Φ_D as it can help say something about the strength of the FAC. As current theories stand, the amount of open flux should be the same in both polar caps at all times. Comparing the amount of open flux in the two polar caps can then tell us something about the quality of fit. Figure 3.1 shows the variations in the flux content for the two polar caps 23/06/15. In that interval there are PCEPs and FCEs for both large and small polar caps, as well as times with high and low dayside reconnection rates. On average it can be seen that polar caps follow each other quite well, but there are "spikes" where one of the OCBs probably has been wrongly determined. It can also be seen that, as expected, the determination creates a more unstable result for large polar caps. For times with a large polar cap, a small miss in the OCB will lead to larger misses in the open flux content then for times with a small polar cap.

Interestingly, there are several intervals where one of the polar caps is consistently larger than the other. One such interval can be seen between 20:45 – 22:15 UT in figure 3.1. Here the southern polar cap is on average 0.2 GWb larger than the northern polar cap for 1.5 h. There is a couple of possibilities as to why this happens. One possibility is that the fit for the Region 1 Birkeland current tracks different sheets of plasma in the two hemispheres. In theory there should only be FAC at two locations, the OCB (Region 1 Birkeland current) and at the polar oval (Region 2 Birkeland current). In reality though, the picture is much more complex. Looking at the plot of the FAC data in figure 4.1, right panel, one can see up to five locations with FAC for some local times. If that is the case in both hemispheres, then the fits might chose differently leading to the observed differences. 2) There is also the possibility that an asymmetry between the polar caps exists. Both 1) and 2) are fields of study, so we will just have to wait to see what answers the future holds.

The strength of the FAC will also determine how good the fit for the OCB is, or whether the OCB can be found at all. Weak FACs are probably the reason for most of missing data points, as there is a cutoff for how weak the FAC can get before the OCB cannot be determined Clausen et al. (2012). The FACs themselves are determined by reconnection rates, so high dayside reconnection rate should stabilize the determinations and a weak reconnection rate should produce more fluctuations in the fit. Figure 4.1 shows plots of FACs in the northern hemisphere for two different times. A) is a time where $\Phi_D = 0$ and has mostly been zero, northward IMF, the last few hours. With a small polar cap, $F_{PC} \approx 0.5$GWb. In contrast is B) during one of the strongest periods of activity observed in Φ_D. F_{PC}

at B) is also one of the largest found, at around 1.1GWb. Both times corresponds to a local maxima in F_{PC} followed by a short FCE. Looking at those two times one can clearly see that for high activity periods (like B)) the FAC creates an oval. In contrast, times with low intensity like A) does not produce a clear oval. One should therefore expect more missing data point around A) then B), as the fit should struggle more here. That is however not clearly reflected in the data, as there is close to equally many missing data points around both times. It is possible that either more ACE or more AMPERE data is missing around B) then A), but I do not have the data to say whether that is the case or not.

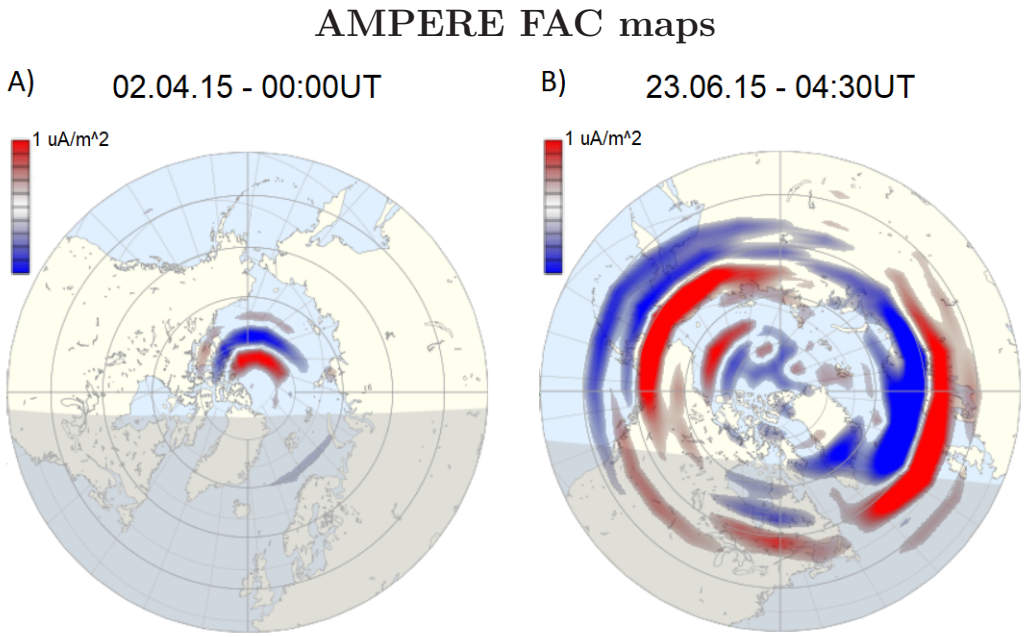

Figure 4.1: Field aligned current over the northern hemisphere for 02.04.15 00:00UT A) and 23.06.15 04:30UT. A) corresponds to low activity in Φ_D, whilst B) is corresponds to high activity. Plots are obtained from http://ampere.jhuapl.edu/products/plots/index.html

Looking back at figure 3.1 and figure 3.3 we can see that 09:00-12:00 UT corresponds to a high dayside reconnection rate, resulting in well-behaved flux determinations, whilst in contrast 15:00 – 18:00 UT shows a low dayside reconnection rate and rapid fluctuations in the flux determinations. Low reconnection rates can be ruled out as a reason for the differences in the polar caps for the shaded areas in figure 3.1, as Φ_D is of considerable sizes there being close to 50 kV thought the last interval. In the end I take the average of the two polar caps, to minimize the various instabilities in the determination of the polar cap size. This seems to work well for most times, smoothing out fluctuations in the polar caps and reducing faults where one of the polar caps is wrongly determined. My remaining concern are those times with consistently different polar caps. Looking at the first shaded area in figure 3.1 one can see that a FCE starts just before and ends at the start of the shaded area. It ends there because the northern polar cap suddenly increases there, but at the same time the southern polar cap shrinks further. So should the FCE end at the start of this interval like northern polar cap suggest or should it continue like southern polar cap suggest? Similarly, for the last shaded area in figure 3.1, should the FCE start from a large value (southern) or a low value (northern)? I do not know if taking the average is the best thing to do, but it is the best choice I can see, as I cannot confirm which or if both polar caps are correct. All I can say is that this affects the determination of F_{PC}, and that will in turn affect the correlation I do.

The smoothing and missing data

After finding the average of the polar caps there still remains a "noise" in the data. So to smooth out these rapid fluctuations, and further reduce the error from wrong determinations, I apply a time smoothing to the average. That smoothing does unfortunately bring with it two possible sources of errors. 1) As the data points are not equally spaced in time will my smoothing be wrong around large gaps in the data. But the effect is at least localized to the eight closest data points. 2) As also pointed out by (Hubert et al., 2006), a time smoothing will have some difficulties following rapid changes. An example of that can be seen in figure 3.2 at about 02:00 UT where the smoothed function F_{PC} does not follow the average all the way down in the minimum. This cuts the FCE short, possibly causing fits to underestimate the nightside reconnection rate.

The gaps in the data can also affect the correlation more directly. As the attempted fits in points before a gap will behave as the next "missing" point were on straight line between the point before and the point after the gap. If the "missing" point is not on that line, which is likely, then a wrong fit will be preferred over the "correct one". Worse yet, due to the fact that an integration is done before the correlation, the fits will be weighted towards the point before gaps. Mitigating this effect is therefore important to get a reliable result. My attempt at this is to simply end a FCE if a gap of 15 min or more starts. I should possibly have brought this threshold further down, but unfortunately shortening the FCEs will have an adverse effect of falsely bringing the PCC up, since many short FCE will have higher PCC by default than a few long ones. As F_{PC} and F'_{pc} will be given the same value at the start of every FCE (see figure 3.6), the PCC will increase when the FCEs are split into multiple short FCEs. Raising the PCC artificially in this way will, as far as I can tell, not make the fitting process choose the wrong parametrization within a given Method. However, it will be more difficult telling how good the best result is.
I also ran the program without the threshold, then with gaps lasting up to 10 h. The differences seen for that was lower PCC values, slight changes in $\alpha, \beta, \gamma, \delta$, longer time shifts (especially for IMF, with an extra $10\mathrm{R_E}$) and Method 2 was over all the best. Things like choice of angle, $\vec{B}$-component and inclusion of flux remained the same. The relatively small changes I observed by implementing a threshold, gives me hope that this is not a large source of error.

The dayside reconnection rate

Before I looked at Φ_D, I planned to use equation 1.2 to find what Φ_N needed to be and correlate directly to that. However it immediately became clear that Φ_D was too small in many data points, prompting Φ_N to be negative, which it cannot be. Figure 3.3 shows some of this behavior, places where the polar cap clearly grow and $\Phi_D = 0$. Therefore I only correlate during FCEs, as I know the required Φ_N must be positive there. Limiting the correlation to FCEs also gave rise to Method 1, as it would not be possible outside the FCEs.

Φ_D is of course zero for northward IMF, because I set it to zero there. That is however not the only reason for it to be too small. The function that Milan et al. (2012) finds is sharply dependent on the direction of the IMF, dropping off fast when the IMF moves away from being purely negative. That dependence is in it of itself not surprising, as Milan et al. (2012) chooses growth phases where the IMF is southward. So as it stands, Φ_D should really be improved and this correlation done anew. I believe that Φ_D needs an explicit function of B_Y in addition to the function found by Milan et al. (2012). That would counteract the weak reconnection around $\theta = \pi/2$ and allow for a dayside reconnection for northward IMF. I am not alone in pointing out this dependency on B_Y as Hubert et al. (2006); Lockwood et al. (2016) and more also notes the B_Y contribution. There is also the question of seasonal dependencies, but these are found to be negligible Lockwood et al. (2016).

Being too small is not the only problem with Φ_D size, there are also times where Φ_D is too large. Multiple studies have shown that the cross polar cap potential has an upper limit, and as the cross polar cap potential equals the sum of nightside and dayside reconnections must Φ_D also have an upper limit. The value of that limit, for the cross polar cap potential, is as of yet not certain. Different studies give different results depending on the measurements used, but all place it way below the values seen in figure 3.3. Most studies seem to give a value somewhere between 100 and 200 kV (Shepherd, 2007).
Milan et al. (2012) also points out a problem, which will affect my correlation. When looking at the predicted arrival times of the solar wind at the magnetopause obtained from OMNI data and compare

that with SYM-H index and solar wind shocks, they find that there is a discrepancy between the actual arrival times and the predicted ones. To combat that problem they time shift their data appropriately, for the worst interval they look at that corresponds to 20 min. I have not dealt with this problem in any way, as manually choosing FCE interval and correctly time shifting them would take time and data I do not have. So in the end I am just hoping that this is not as serious for my intervals. Also, a space weather model probably could not have done this anyway.

I also would like to point out that Milan et al. (2012) leaves out one question. Is the found function for dayside reconnection valid outside of growth phases? Milan et al. (2012) ends the correlation the moment there are signs of nightside reconnection happening. When the nightside reconnection gets going we expect to see increased convection, t_7 in figure 1.2. Will that change the shape of the magnetopause? If so, will the area where magnetic reconnection takes place change? That would change the scale factor used by Milan et al. (2012). Will reconnection site/s be the same when flux flows towards the dayside on the dusk and/or dawn sides? Will the dependency on B_Y change if geomagnetic field lines away from the noon-midnight line becomes more involved? Will this give a response in the clock angle dependency?

4.2 The results

One of the prerequisites for Φ_N is that it should tend to zero during PCEPs. If it does not, it will contradict countless observations and bring the validity of Φ_D into doubt as it assumes this. Sadly, one thing becomes immediately clear when the two parametrizations are plotted as functions of time; they do not tend to zero during PCEPs. This tell me that neither of the parametrizations can be used indiscriminately as they are. However, they are good during FCEs so I believe they would work well if some sort of trigger and stopping criteria is found.
Assuming that such criteria can be found, then it is seen from figure 3.7 that both parametrizations on average behave well and match the quality of Φ_D. For reference the PCC value for Φ_D as used comes out as 0.784 when correlating with the PCEPs in the data. Ignoring PCEPs where the IMF if northward brings the PCC up to 0.876. So Φ_D is overall worse than both my functions, but on par under circumstances similar too that it assumes. Inferring from Hubert et al. (2006) that the nightside reconnection rate can begin before we see a reduction in F_{PC} and knowing from table 3.5 that both parametrizations underestimate Φ_N in most of the FCEs 18/10/15, should result in an overestimation of F_{PC} at the end of the time interval shown in figure 3.7. However both lead to an underestimation. This is just further evidence that Φ_D is not entirely correct. In turn this also directly effects result in Method 2, as it uses Φ_D in the correlation. I believe that it is this extra uncertainty that Φ_D introduces that makes Method 2 worse than Method 1 in terms of correlation.

Similarities and Differences

Both methods choose B_{YZ} as the best IMF component. This also falls in line with Φ_D which puts B_{YZ} as the most important IMF component in determining how much flux that enters the tail lobes. This interpretation can possibly continue on for Method 2, and be interpreted as field lines "pushing" each other over the polar cap toward the nightside reconnection site. This would then explain the short time shift in the IMF parameters, as it might be a time shift in to the magnetopause where the dayside reconnection happens. Method 1 has the opposite angle dependency, so for that function the interpretation may be that the solar wind hits the magnetopause at the tail lobes and push the tail lobes together. This would again explain the observed time shift in the IMF parameters for that function. So possible physical interpretations exist for the found functions, but I do not put much faith in that and only think of these parametrizations as something that works.

Another thing that the methods has in common is a weak inverse dependency on N_p. In truth is this a bit baffling, as I would expect more activity at times with a dense SW. However, that expectation stems from the fact that dense SWs often carries stronger magnetic fields with it. So this dependency might be there to avoid saturation, as the cross polar cap potential is still limited. It is also possible that the parametrizations simply uses N_p because it can. Regardless the reason I do not believe this dependency belongs in the parametrization as the underestimations in figure 3.6 corresponds to strong N_p, and weakening the parametrizations at those times is clearly the wrong thing to do.

As the parametrization from Method 2 is now, it has a weak dependency on the clock angle with a maximum for southward IMF. That dependency is there because the parametrization needs to be big when there is ongoing dayside reconnection. A larger Φ_D when the IMF is northward would then weaken that dependency, possibly getting rid of it altogether. Method 1 has a dependency on reverse clock angle, but this is also weak as with Method 2. I believe this dependency might be there because the IMF is mostly northward pointing during the FCEs used in the correlation. So it might be something that is due to the correlation interval chosen, and another interval might give something different. In which case it might also be independent of angle, but I have not had time to test this. As seen from figure 3.4, this would bring the PCC down so much that several of the other parametrization would outcompete it, at least within the chosen interval. If this northward dependency truly is there, then a question would be; how does this effect the phenomena now as lobe reconnection. Lobe reconnection is when strongly northward IMF reconnect with both tail lobes and close magnetic flux on the dayside. I have chosen to ignore lobe reconnection, as it is found to only be relevant for sharply northward IMF and even then is the total amount of flux closed small (Imber et al., 2006).

Method 1 is contrary to Method 2 not dependent on Φ_D in the correlation, and I believe this is the deciding factor that makes Method 1 perform better. And since I do not see any clear performance differences, it is this function (equation 3.2) I would go with, being careful with trusting it during dense SW (10 cm^{-3} and up), and keeping an eye on the angle dependency. The question is then: is this better than Method 2 for a space weather model? Sadly the answer is, probably not. As it is the cross polar cap potential that is needed in equation 1.5 to calculate the electric potential on the adiaroc lines, and that would be

$$\Phi_{PC} = \Phi_N^* + 2\Phi_D$$

So the uncertainty in Φ_D will haunt Method 1 as well. In any case is all of this dependent on finding a trigger for the FCEs. At that has all my attempts failed, so this is left to someone else.

4.3 The possibility for a probabilistic function for Φ_N

I also briefly looked into whether a statistical approach to find Φ_N would work. However, due to the time restraints on this thesis and disconcerting results in the literature, I chose to focus on a parametrization based mainly on the IMF characteristics. I will however give a short summary of my thoughts around a statistical approach for Φ_N. As with today's weather forecasts, the calculation of Φ_N would require one or more parameters describing the current situation. From the current situation, the most probable function for nightside reconnection would be calculated. Where the calculation would use probabilities attained by a statistical analysis of the time interval 2010 - mid 2017. The analysis should give a probabilistic correlation between the input parameters and observed change in open flux.

Since I do not see a steady decline in the amount of open flux outside of FCEs, I would probably do as Milan et al. (2012) and say that $\Phi_N = 0$ outside the FCEs. As I see it, this leaves three things to account for in the description of Φ_N:

1) An estimate for the FCE onset time.

2) A stopping criteria for the FCE, i.e. a duration for that particular FCE, or perhaps stopping it after a certain amount of flux have been closed.

3) A description of the time evolution for Φ_N, between onset and the end of the FCE.

The third criteria might be the easiest to solve. A semi-probabilistic function like either Method 1 or Method 2 can be used here, and the list is reduced to points 1) and 2). Alternatively one can go for a fully probabilistic function to see if that can approximate the physical system. Looking at the time changes in the open flux one can see that Φ_N begins at small values and increases to a peak before it decreases to zero again. Possible functions can be a half period sinusoidal, a Gaussian or a parabola. The problem would lie in determining an amplitude for the function. The amplitude would have to be a function of the input parameter/s in some way, it is not unlikely that this function also would have some probabilistic element. Alternatively the amplitude could be determined if we had both the duration and an estimate for how much flux that are closed during that FCE. However, this would only shift the problem from having to fulfill two criteria for 2), to instead having to fulfill one criteria for 2) and one for 3).

What parameter/s to choose?

One possible choice is the total amount of open flux within the polar cap F_{PC}. There are a couple of things that make F_{PC} an attractive choice, most importantly we already know that F_{PC} is connected/related to Φ_N through equation 1.2, which tells us the expected behavior of F_{PC} in regards to Φ_N. Another advantage with F_{PC} is that, through the estimate for dayside reconnection rate provided by Milan et al. (2012), we from IMF parameters can predict open flux input to F_{PC}. So one would think that it is possible to estimate the nightside reconnection rate from F_{PC}. Not that surprisingly, some preliminary exploration into this has already been done in the literature, and the results are not that encouraging.

FCE onsets have not been specifically studied, but substorm onsets have. Since substorms in terms of reconnection rates can be thought of a as a subcategory of FCEs, namely FCE that releases so much energy that it creates magnetic substorms, it should give some insights in FCE onset. Boakes et al. (2009) attempted to determine the probability of substorm onset as a function of F_{PC}. They identified substorms in December 2000, 01, 02 and January 2001 & 02 (five months in total), using the method described by Frey et al. (2004). For the same interval auroral images from the IMAGE satellite are used to estimate the OCB and calculate F_{PC}, assuming the Earth's magnetic field to be a dipole. In total they are able determine F_{PC} for 173 substorm onsets using this method. From that it is found that the probability for substorm onset increases linearly with F_{PC}. Estimating an onset based on that means that the space weather model would be prone to many wrong onsets, both too early and too late. A sharp trigger is needed, which would manifest as a localized high probability.

Observed onsets

That the probability for substorm onset based on F_{PC} is not helpful, does not necessarily rule out that the probability for FCE onsets can be based on F_{PC}. So I attempted to redo Boakes et al. (2009) analysis for FCEs instead of substorms. To do that I keep F_{PC} as stated section 2. The derivative is changed to be the slope of the best linear fit through 3 points in F_{PC}. This is sort of a second smoothing, done to keep the derivative from needlessly starting a new FCE if it is positive in a single point like shown in figure 3.6. After that the FCE intervals are identified in just the same way. The distribution of onsets, the first points in the FCEs, is seen in figure 4.2.
The probability for the FCE onset seems be fairly constant, indicating no dependency on F_{PC} when one looks at the bottom right plot in figure 4.2. I think this is mostly due to onsets which really are not onsets at all, and that my second smoothing was not effective enough. So in an attempt to only pick out true FCE onsets that also corresponds better with Boake's analysis, I pick out the onsets that occur following a southward turning (B_Z going from positive to negative) of the IMF if it is within 2 h of the turning. If several southward turnings are observed between onsets only the first succeeding onset is chosen (if it is within 2 h). This is of course not a perfect way of doing things, but the method should be closer to Boakes et al. (2009). A Gaussian shape can now be seen for the onset probability in the top right plot in figure 4.2. It is however far from the sharp value is needed. The reality seem to be mostly the same as Boakes et al. (2009) found for substorms, FCEs can occur for any size of F_{PC}. In complete agreement with Boakes et al. (2009) is the onset probability zero below 0.3 GWb, but that is because F_{PC} never drops below this value. The sharp increases above 1.1 GWb is probably due to too little data, but can be true.

I also tried the dynamic solar wind pressure p_d, the product of p_d and F_{PC} and the sizes of Method 1 and 2, but none of these gave any sensible results. So I believe that if it is possible to estimate FCE onsets from the available data, then a more complex conditional probability must be used. Simple models for onset, probabilistic and physical, have been searched for, a long time but none has been found. Likely one needs to use something that describes the internal processes in the tail to get a correct result.

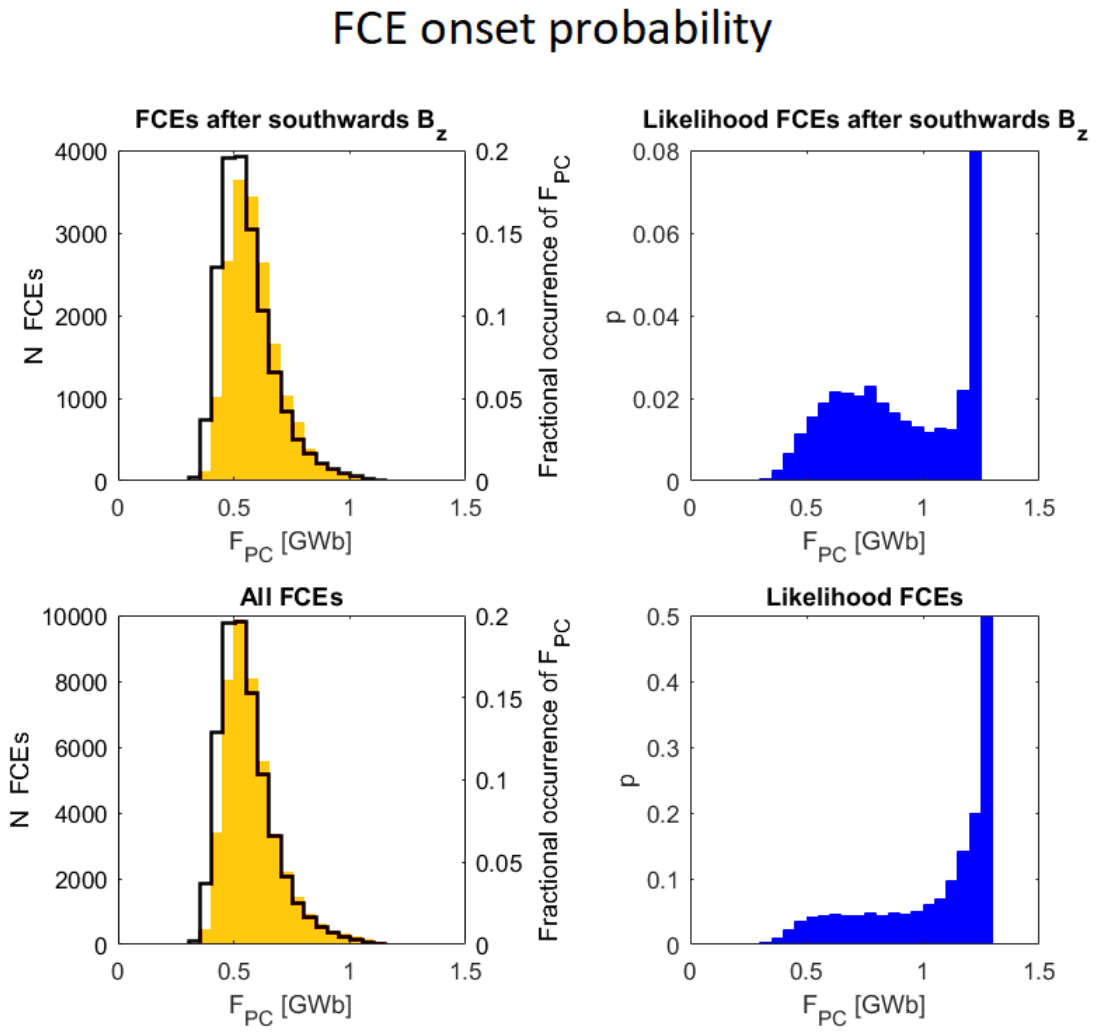

Figure 4.2: The left column shows the distribution of FCE onset as a function of F_{PC} (in filled bars). The black line is the fractional occurrence of F_{PC} ($\#F_{PC}$/ total number of data points) within intervals of 0.05 GWb. The top row only includes FCEs following a southward turning of the IMF, and the bottom row shows the same results when all FCEs is included. The right column shows the probability of a FCE onset within those intervals of F_{PC} (N FCEs / $\#F_{PC}$). Using data from 01/01/10 - 01/07/17.

CHAPTER 5

Summary

5.1 Summary and the road ahead

In this work, I have attempted to parametrize the nightside reconnection rate using the open magnetic flux in the polar caps and IMF parameters. In order to do this, I have performed a correlation analysis between several parametrizations and the observed changes in the open magnetic flux contained within the polar caps, during times of contracting polar caps. I find that net-closure rate of open flux can be well described as:

$$\Phi_N^* = 7.018 \cdot 10^5 \cdot F_{PC}(t - 22.0\text{min}) B_{YZ}^{0.295} v_T^{0.420} N_p^{-0.121} \sin^{0.314}\left(\frac{1}{2}(\pi - \theta)\right)$$

with the IMF parameters time shifted to $k = -1.5\text{R}_\text{E}$. This works best for times with low SW densities, below 10 cm^{-3}, as it is seen that this parametrization tends to underestimate for dense SW. The parametrization is also only valid during times with contracting polar caps. Therefore, some criteria for the start and end of these intervals have to be found to use it.

I also find that nightside reconnection rate can be reasonably well described as

$$\Phi_N = 2.639 \cdot 10^6 \cdot F_{PC}(t - 16.0\text{min}) B_{YZ}^{0.520} v_T^{0.712} N_p^{-0.159} \sin^{0.302}\left(\frac{1}{2}\theta\right)$$

with the IMF parameters time shifted to $k = 12\text{R}_\text{E}$. With the same problems for N_p, as well as start and stopping criteria. This does not correlate as well with the observed changes in F_{PC} as the net-closure rate, something I contribute to the extra uncertainty introduced by Φ_D. I feel that with a proper Φ_D, equation 2.5 should produce a Φ_N that gives a better correlation than equation 2.4. I therefore wish for a more comprehensive study of the dayside reconnection rate that answers the following questions:

1) Is there a larger dependency on B_Y for clock angles around $\pi/2$ than that found by Milan et al. (2012)?
2) When does Φ_D need to be caped off due to saturation of polar caps?
3) Is the description for the dayside reconnection rate different for high and low solar wind densities?
4) Does the found Φ_D describe the dayside reconnection rate at both times with and without nightside reconnection?

With a Φ_D in place the correlation can be redone for Φ_N, and the same questions can tackled for Φ_N . As well as the seemingly most difficult question: what determines the onset of the flux closure events?

Appendices

APPENDIX A

The Pearson product-moment correlation coefficient

Calculating the Pearson correlation coefficient (PCC) is a way of comparing two sets of data, to determine whether there is a correlation between them. This is done by calculating the covariance of the data sets X and Y, and dividing by their standard deviations σ_X and σ_Y.

$$PCC = Corr(X, Y) = \frac{\text{Cov(X,Y)}}{\sigma_X \cdot \sigma_Y} \tag{A.1}$$

The PCC always assumes a value between -1 and 1, with 1 meaning a perfect positive correlation (X and Y increases together), 0 no correlation or constant values and -1 a perfect negative correlation (X increases and Y decreases or vice versa). The geometric interpretation of this is that a plot of Y against X will form a straight line for $PCC = 1$ and $PCC = -1$, whilst 0 will give "chaos". This means that the PCC can be used as a measure of how good a parametrization is at following the changes in that which we want to parametrize, but that which truly makes it worth while to use is the following proposition:

$$Corr(aX + b, cY + d) = Corr(X, Y) \tag{A.2}$$

This states that the PCC is not affected by a linear change in the units of measurement, meaning that the parametrization does not need to be correctly scaled or have the correct constant term. This makes the PCC to an incredible powerful tool, but one must be aware that a high PCC do not necessarily prove a causial link between between X and Y. That will still have to be argued separately. (Devore and Berk, 2012)

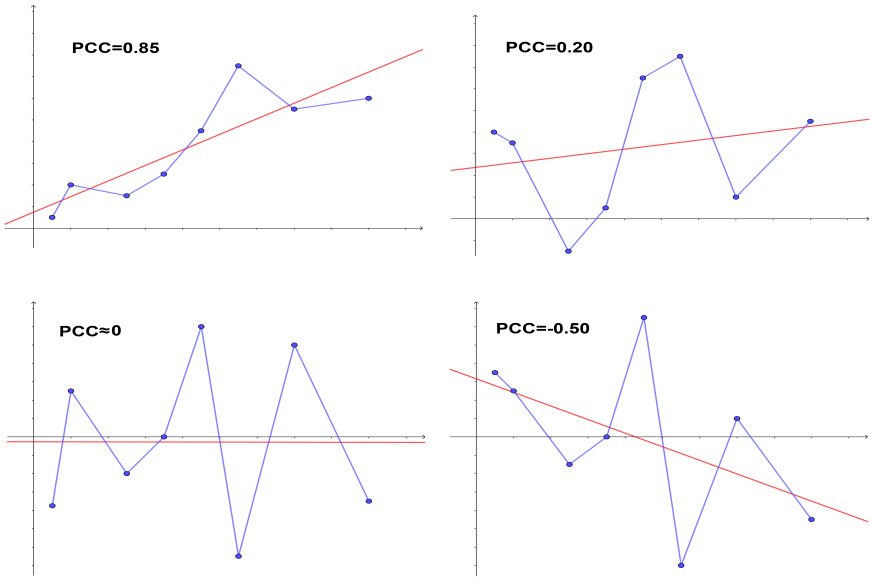

Figure A.1: Some examples showing the geometric interpretation of the Pearson correlation coefficient for some given values

Bibliography

Akasofu, S.-I. The development of the auroral substorm. *Planetary and Space Science*, 12:273–282, April 1964. doi: 10.1016/0032-0633(64)90151-5.

Boakes, P. D., Milan, S. E., Abel, G. A., Freeman, M. P., Chisham, G., and Hubert, B. A statistical study of the open magnetic flux content of the magnetosphere at the time of substorm onset. *Geophysical Research Letters*, 36:L04105, February 2009. doi: 10.1029/2008GL037059.

Clausen, L. B. N., Baker, J. B. H., Ruohoniemi, J. M., Milan, S. E., and Anderson, B. J. Dynamics of the region 1 Birkeland current oval derived from the Active Magnetosphere and Planetary Electrodynamics Response Experiment (AMPERE). *Journal of Geophysical Research (Space Physics)*, 117:A06233, June 2012. doi: 10.1029/2012JA017666.

Clausen, L. B. N., Baker, J. B. H., Ruohoniemi, J. M., Milan, S. E., Coxon, J. C., Wing, S., Ohtani, S., and Anderson, B. J. Temporal and spatial dynamics of the regions 1 and 2 Birkeland currents during substorms. *Journal of Geophysical Research (Space Physics)*, 118:3007–3016, June 2013. doi: 10.1002/jgra.50288.

Cowley, S. W. H. and Lockwood, M. Excitation and decay of solar wind-driven flows in the magnetosphere-ionosphere system. *Annales Geophysicae*, 10:103–115, February 1992.

Devore, J. L. and Berk, K. N. *Modern Mathematical Statistics with Applications*. Springer New York Dordrecht Heidelberg London, second edition edition, 2012.

Dungey, J. W. Interplanetary Magnetic Field and the Auroral Zones. *Physical Review Letters*, 6: 47–48, January 1961. doi: 10.1103/PhysRevLett.6.47.

Frey, H. U., Mende, S. B., Angelopoulos, V., and Donovan, E. F. Substorm onset observations by IMAGE-FUV. *Journal of Geophysical Research (Space Physics)*, 109:A10304, October 2004. doi: 10.1029/2004JA010607.

Hubert, B., Milan, S. E., Grocott, A., Blockx, C., Cowley, S. W. H., and GéRard, J.-C. Dayside and nightside reconnection rates inferred from IMAGE FUV and Super Dual Auroral Radar Network data. *Journal of Geophysical Research (Space Physics)*, 111:A03217, March 2006. doi: 10.1029/2005JA011140.

Imber, S. M., Milan, S. E., and Hubert, B. The auroral and ionospheric flow signatures of dual lobe reconnection. *Annales Geophysicae*, 24:3115–3129, November 2006. doi: 10.5194/angeo-24-3115-2006.

Lockwood, M. and Cowley, S. W. H. Ionospheric convection and the substorm cycle. *Proceedings of the International Conference on Substorms (ICS-1)*, pages 99–109, 1992.

Lockwood, M., Owens, M. J., Barnard, L. A., Bentley, S., Scott, C. J., and Watt, C. E. On the origins and timescales of geoeffective IMF. *Space Weather*, 14:406–432, June 2016. doi: 10.1002/2016SW001375.

McPherron, R. L., Russell, C. T., and Aubry, M. P. Satellite studies of magnetospheric substorms on August 15, 1968: 9. Phenomenological model for substorms. *Journal of Geophysical Research (Space Physics)*, 78:3131, 1973. doi: 10.1029/JA078i016p03131.

Milan, S. E., Gosling, J. S., and Hubert, B. Relationship between interplanetary parameters and the magnetopause reconnection rate quantified from observations of the expanding polar cap. *Journal of Geophysical Research (Space Physics)*, 117:A03226, March 2012. doi: 10.1029/2011JA017082.

Misra, P. and Enge, P. *Global Positioning System: Signals, Measurements, and Performance*. Ganga-Jamuna Press, Lincoln MA, revised second edition edition, 2010.

Østgaard, N., Moen, J., Mende, S. B., Frey, H. U., Immel, T. J., Gallop, P., Oksavik, K., and Fujimoto, M. Estimates of magnetotail reconnection rate based on IMAGE FUV and EISCAT measurements. *Annales Geophysicae*, 23:123–134, January 2005. doi: 10.5194/angeo-23-123-2005.

Pécseli, H. *Waves and Oscillations in Plasmas*. CRC Press Inc, September 2012. doi: 10.1201/b12702.

Petrinec, S. M. The location of the Earth's bow shock. *Planetary and Space Science*, 50:541–547, April 2002. doi: 10.1016/S0032-0633(02)00033-8.

Prölss, G. W. and Bird, M. K. *Physics of the Earth's Space Environment: An introduction*. Springer-Verlag Berlin Heidelberg, 2004.

Russell, C. T. and McPherron, R. L. The Magnetotail and Substorms. *Space Science Reviews*, 15: 205–266, November 1973. doi: 10.1007/BF00169321.

Shepherd, S. G. Polar cap potential saturation: Observations, theory, and modeling. *Journal of Atmospheric and Solar-Terrestrial Physics*, 69:234–248, March 2007. doi: 10.1016/j.jastp.2006.07.022.

Siscoe, G. L. and Huang, T. S. Polar cap inflation and deflation. *Journal of Geophysical Research (Space Physics)*, 90:543–547, January 1985. doi: 10.1029/JA090iA01p00543.

Waters, C. L., Anderson, B. J., and Liou, K. Estimation of global field aligned currents using the iridium® System magnetometer data. *Geophysical Research Letters*, 28:2165–2168, 2001. doi: 10.1029/2000GL012725.